Supplementary information

for

Unveiling autophagy and aging through time-resolved imaging of lysosomal polarity with a delayed fluorescent emitter

Subhadeep Das, Abhilasha Batra, Subhankar Kundu, Rati Sharma, and Abhijit Patra*

Department of Chemistry, Indian Institute of Science Education and Research Bhopal,

Bhopal Bypass Road, Bhauri, Bhopal 462066, Madhya Pradesh, India

Email: abhijit@iiserb.ac.in

I. Materials and methods

1.1 Chemicals:

4-Bromo salicylaldehyde (97%), diethyl malonate (synthesis grade), diphenylamine (99%), *N*, *N*'-dicyclohexylcarbodiimide (DCC, 99%), hydroxybenzotriazole (HOBt, 97%), tris(dibenzylideneacetone) dipalladium (0) (99%), 4-dimethylaminopyridine, XPhos (99%), calcium carbonate (99%), carbonyl cyanide *m*-chlorophenyl hydrazone (CCCP, 97%), polyvinyl alcohol (13 - 27 KDa, 87 - 89% hydrolysed), polystyrene (280 KDa), autophagy assay (MAK138), deoxy D-glucose, chloroquine, lipopolysaccharide (LPS) *Escherichia coli* K-235, and toluene (99.8%) were collected from Sigma-Aldrich Chemicals Pvt. Ltd. Solvents for spectroscopy and synthesis like ethanol (99.8%), toluene, hexane, acetonitrile, tetrahydrofuran, chloroform, dichloromethane (DCM) and dimethyl sulfoxide (DMSO) were collected from Spectrochem. LysoTracker™ Green, LysoTracker™ Red, MitoTracker™ Green, CellMask™ Green, 4',6-diamidino-2-phenylindole (DAPI), BODIPY 493/503, SYBR Green I, propidium iodide (PI), Dulbecco's modified Eagle's medium (DMEM), phosphate-buffered saline (PBS, 1X), trypsin-EDTA solution (0.25%), fetal bovine serum (FBS), FluoroBrite™ DMEM, 3-(4,5-dimethylthiazol-2-yl)-2,5-diphenyltetrazolium bromide (MTT) and penicillin-streptomycin-glutamine (PSG 100X) were collected from ThermoFisher Scientific. Amiloride and chlorpromazine were purchased from the Tokyo Chemical Industry.

1.2 Instrumentation:

Characterizations of all the synthesized compounds were performed using Brucker Avance III nuclear magnetic resonance (NMR) spectrometer (500 MHz) and Bruker MicrOTOF-Q-II mass spectrometer. Jyoti melting point detector (ISO: 9001:2000, India) was used for measuring the melting points of the compounds.

Agilent Cary 100 spectrophotometer and Jobin Yvon Horiba Model Fluorolog-3-21 (450 W Xe lamp) were used to record the UV-visible absorption and fluorescence spectra of the solutions and nanoparticles, respectively. Edinburgh LP980 fluorescence spectrometer was used for the laser fluence-dependent measurements of the probes. Unless stated otherwise, the concentration of DC-Lyso used for spectroscopic measurements was taken as 2 μM.

The excited state lifetime of the samples was measured using a Delta Flex-01-DD/HORIBA spectrometer. DeltaDiodes of 408 nm, 470 nm, and SpectraLED of 417 nm and 461 nm were used as excitation sources, and Ludox was used to record the instrument response function (IRF) for each case. The decay spectra were fitted using Horiba EzTime software considering the fitting parameter (χ^2). Time-resolved emission spectra (TRES) were recorded within the wavelength range of 450 - 800 nm (wavelength interval = 3 - 5 nm).

The aqueous dispersion of DC-Lyso, *i.e.*, DCL-NPs, was prepared by adding 30 μL of DC-Lyso (1 mM) in 3 mL of 90% water-DMSO solvent mixture (1 min sonication). The pure aqueous dispersion of DC-Lyso, *i.e.*, DCL-100, was prepared by adding 6 μL of DC-Lyso (1 mM) in 3 mL

of water (1 min sonication). The morphology of the nanoparticles was visualized through an FEI TALOS 200S transmission electron microscope (TEM, working voltage: 200 kV). The samples for TEM were prepared by drop-casting the dispersion (~10 μL) of the nanoparticles over a 200 mesh Cu grid. The samples were dried under a vacuum overnight before imaging.

Fluorescence quantum yield: Coumarin-153 in ethanol (Φ_f = 53%) was used as a reference dye for estimating the fluorescence quantum yield (Q.Y.) of DC-Lyso following the Eqn. S1.[1]

$$\Phi_f = \Phi_{f,s} \times \frac{F_X}{F_s} \times \frac{f_s}{f_x} \times \frac{n_X^2}{n_S^2} \quad \text{..... (Eqn. S1)}$$

$$f = 1 - 10^{-A_{\lambda ex}} \text{..... (Eqn. S2)}$$

Where, n, F, and Φ are the refractive index, integral fluorescence, and fluorescence quantum yield, respectively, where the subscripts s and x refer to the standard and sample, respectively. λ_{ex}, ε, and A denote the excitation wavelength, molar extinction coefficient (L mol^{-1} cm^{-1}), and absorbance, respectively.

Fabrication of DC-Lyso-doped thin films: Thin films of DC-Lyso (1 wt.%) in polystyrene (PS) and polyvinyl alcohol (PVA) were fabricated through spin coating (1000 rpm, 2 min) methanol solution on a quartz plate, followed by drying under vacuum.

Fluorescence microscopy: Mammalian cells were imaged using a Zeiss Axio Imager M.2 Apotome microscope. PicoQuant, MicroTime 200 clubbed with Olympus IX-73 (inverted optical microscope) was used for intracellular photostability, fluorescence imaging, lysosomal dynamics, and fluorescence lifetime imaging microscopy (FLIM) of biological samples using the time-tagged time-resolved (TTTR) mode.[2]

Cell culture: Mammalian cells were cultured in tissue culture dishes (Tarsons, 60 mm) with phenol red containing DMEM, supplemented with 1% (v/v) PSG and 10% (v/v) FBS under humid conditions, *i.e.*, 5% CO_2, 37 °C. The grown cells were trypsinized and transferred to confocal dishes (SPL life sciences, 10 mm) before 24 h of imaging. Then, PBS was used to wash the cells thrice, and the dye-containing DMEM (2 mL) was added to the confocal dishes. The cells were incubated with DC-Lyso (2 μM) for 10 min, if not mentioned otherwise. The incubation time for DCL-NPs (2 μM) for imaging was 10 min. The commercial tracker dyes (0.5 μM) were incubated for 5 min in humid conditions before imaging, if not mentioned otherwise. After the probe incubation, PBS was used to wash the cells thrice, and FluoroBrite™ DMEM (2 mL) was added for imaging.

MTT assay: In 96-well plates (Nunc, ThermoFisher), HeLa cells were seeded with a cell density of ~10^6 cells per well under humid conditions. After 24 h, the grown cells were treated with different concentrations of DC-Lyso or DCL-NPs and incubated again for 24 h. Thereafter, the cells were washed thrice with PBS and then incubated with MTT solution (10 v/v % of DMEM, conc. 2 mg mL^{-1}) for 1.5 h. Discarding the media, the formazan crystals were dissolved in DMSO

(100 µL). After rocking the plate for 20 min, absorbance from each well was recorded at 570 nm using a plate reader (BioTek Instruments Inc, Winooski, VT, USA).

For the multiday MTT assay, HeLa cells were seeded in 12 well plates (Nunc, ThermoFisher, cell density of ~2×10^4 cells per well under humid conditions (37 °C, 5% CO_2). After 24 h, the grown cells were treated with different concentrations of DC-Lyso in 3 mL of complete growth media and incubated for 5 days. After that, the cells were gently washed thrice with PBS and then incubated with the MTT solution (10 v/v % of DMEM, conc. 2 mg mL^{-1}) for 1.5 h. Discarding the media, the formazan crystals were dissolved in DMSO (300 µL). After rocking the plate for 20 min, absorbance from each well was recorded at 570 nm using a plate reader (BioTek Instruments Inc, Winooski, VT, USA).

JC-1 assay: In twenty-four-well plates containing 2 mL of DMEM media, HeLa cells were seeded with approximately ~1×10^5 cells/well for 24 h (5% CO_2, 37 °C). After the growth, the cells were washed with PBS. Thereafter, the cells were incubated with fresh media consisting of DC-Lyso of various concentrations (1 - 10 µM) for 24 h. After incubation, the cells were again washed with PBS thrice. Then, the DC-Lyso-treated cells were incubated with DMEM containing JC-1 dye (2 µM) for 30 min. After the JC-1 treatment, the cells were washed with PBS, trypsinized, and pelleted using centrifugation (Neuation, D06 iFuge, 1000 rpm, 3 min). The pelleted cells were resuspended in PBS (~500 µL) and were analyzed using fluorescence-activated cell sorting (FACS). The fluorescence intensity of each sample was detected by BD FACSAriaTM III [FITC channel (green): λ_{ex} = 488 nm, λ_{em} = 510 - 550 nm; PE channel (red): λ_{ex} = 488 nm, λ_{em} = 580 - 620 nm]. The experiments were repeated three times. The control set of cells was also prepared using the above procedure, which contained the following sets: (i) unstained cells, *i.e.*, cells without DMSO, DC-Lyso, and JC-1 treatment, (ii) untreated cells, *i.e.*, cells treated with JC-1 but not with DMSO and DC-Lyso, (iii) DMSO treated, and (iv) mitochondrial membrane potential disruptor carbonyl cyanide *m*-chlorophenyl hydrazone (CCCP, 50 µM) treated cells for 30 min. The experiment was performed for three independent measurements.

Temperature-dependent incubation: Grown HeLa cells plated in confocal dishes (1000 cells per dish, 10 mm) were first incubated at different temperatures (4 °C, 20 °C, and 37 °C) in complete growth media for 1 h.[3] Then, the cells were treated with DC-Lyso for 10 min under a 5% CO_2 environment. The cells were washed with PBS (2 mL) thrice, and FluoroBrite™ DMEM (2 mL) was added to the cells before imaging using a confocal microscope.

Incubation in the presence of chemical inhibitors: Grown HeLa cells plated in confocal dishes (1000 cells per dish, 10 mm) were first incubated with chemical inhibitors like amiloride (0.5 µM), chlorpromazine (0.5 µM) for 10 min.[3-5] The active transport-mediated cellular internalization was checked in HeLa cells incubated with glucose-deficient DMEM and 2-deoxy-D-glucose (20 mM) for 1 h at 37 °C.[6] After the chemical incubation, the cells were washed with PBS (2 mL) thrice and incubated with DC-Lyso for 10 min at 37 °C. Thereafter, the cells were washed with PBS (2 mL) thrice, and FluoroBrite™ DMEM (2 mL) was added to the cells before imaging using a confocal microscope.

Long-term imaging: To check the long-term imaging ability of DC-Lyso, HeLa cells were first grown in a 10 mm confocal dish (cell density ~1000 cells per well) and incubated with DC-Lyso (2 μM) for 10 min under 37 °C and 5% CO_2 environment. The excess dye was removed by washing the cells thrice with PBS, and fresh DMEM (2 mL) was added. Subsequently, the cells were incubated for 1-4 days separately. On each day, previous media was discarded, cells were washed with PBS (once), and fresh growth media (2 mL) was added to maintain healthy conditions for cell growth. On respective days, the cells were washed with PBS, and FluoroBrite™ DMEM solution was added before imaging.

Samples for autophagy: We have performed an autophagy assay (MAK138, Sigma-Aldrich)[7] to confirm the occurrence of autophagy during the experimental conditions. HeLa cells were first grown in 96 well plates (10^4 cells per well) under 37 °C and 5% CO_2 environment. To induce autophagic flux, the cells were then treated with growth media supplemented with CCCP (10 μM, 5 min incubation) and another set with growth media and LPS (1 mg mL^{-1}, 1 h incubation). The control set of cells was only incubated in growth media. The negative control sets were incubated with either LPS or CCCP in the presence of chloroquine (CQ, 10 μM), an autophagy inhibitor.[8] After incubation, the media was removed, and the cells were washed with PBS thrice. Thereafter, the autophagosome detection reagent working solution (1X, 500 μL) was added to the cells and incubated for 1 h at 37 °C. Then, the cells were washed four times by gently adding 500 μL of wash buffer. The fluorescence images were recorded using an Apotome.2 fluorescence microscope (λ_{ex} = 335 - 383 nm, λ_{em} = 480 - 540 nm).

We first incubated the HeLa cells with DC-Lyso (2 μM, 10 min incubation, 37 °C, 5% CO_2 atmosphere), and after that, the cells were washed with PBS (2 mL) thrice. Then, the cells were treated with 0.2 μM of BODIPY493/503 for 5 min. After the incubation, the cells were washed 5 times with PBS, and FluoroBrite™ DMEM was added before imaging. To induce lipophagy, the cells were first treated with LPS for 1 h, and subsequently, the cells were stained with DC-Lyso and BODIPY 493/503. Similarly, for monitoring the mitophagy process, CCCP (10 μM) was incubated in MitoTracker™ Green and DC-Lyso-treated cells for 5 min. For control sets, the cells were only treated with commercial dye and DC-Lyso. The experiments were performed for three independent measurements.

***Caenorhabditis elegans* (*C. elegans*) staining:** Wild-type (N2 strain) and short-lived mutant [CF1038 strain, *daf-16*(*mu86*)] *C. elegans* were grown on nematode growth media (NGM) plates (60 mm) seeded with *E. coli* OP50 bacteria at 20 °C.[9] Synchronised worms at different stages of their lifespan (L2, L3, day-1 adult) were washed with M9 media and collected in vials. The worm pellet was collected by removing the supernatant after centrifugation at 1500 rpm for 1 min. After this, the worms were incubated with DC-Lyso (2 μM) or DCL-NPs (2 μM) in M9 media for 2 h under mild shaking at room temperature (24 °C). Finally, the worms were washed with M9 media to remove the free probe. For imaging purposes, the worms were transferred to an agarose pad (2%) and immobilised using (5 mM, 10 μL) Levamisole solution. The experiment was performed for three independent measurements.

II. Synthesis and characterizations

2.1.1. Synthesis of P1: 4-Bromo salicylaldehyde (100 mg, 0.5 mmol) and diethyl malonate (85 µL, 0.55 mmol) were dissolved in 10 mL of acetonitrile. Subsequently, a few drops of piperidine were added, and the reaction mixture was refluxed at 80 °C for 6 h. After cooling the reaction mixture, the precipitate was filtered to afford a pale-yellow solid of ethyl 7-bromo-2-oxo-2H-chromene-3-carboxylate (P1) and purified using recrystallization.

^{1}H NMR (500 MHz, $CDCl_3$) δ: 8.47 (s, 1H), 7.54 (m, 1H), 7.47 (m, 2H), 4.41 (q, *J* = 7.1 Hz, 2H), 1.41 (t, *J* = 7.1 Hz, 3H). **^{13}C NMR (126 MHz, $CDCl_3$)** δ: 163.08, 156.15, 155.52, 148.05, 130.51, 129.10, 128.68, 120.43, 118.73, 117.03, 62.41. **HRMS (ESI):** Calculated for $C_{12}H_9BrO_4$ 295.9684 g mol^{-1}, obtained [(M+1)$^+$] 296.9758 g mol^{-1}.

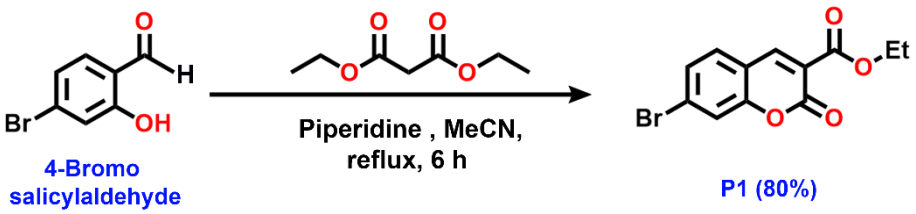

Scheme S1: Synthetic scheme of P1.

2.1.2. Synthesis of P2: To the mixture of P1 (100 mg, 0.34 mmol) in 95% EtOH-water solution, NaOH (84 mg, 2.1 mmol) was added and refluxed for 2 h. After cooling, the reaction mixture was quenched in 20% HCl solution, and the precipitate was washed with water and pentane. The product was purified by recrystallization in 50% EtOH-water to obtain P2 as a yellow solid.

^{1}H NMR (500 MHz, $CDCl_3$) δ: 12.05 (s, 1H), 8.90 (s, 1H), 7.69 (s, 1H), 7.62 (d, *J* = 8.3 Hz, 2H). **^{13}C NMR (126 MHz, $CDCl_3$)** δ: 163.39, 162.03, 154.52, 150.73, 131.16, 130.60, 129.94, 120.65, 117.31, 115.04. **HRMS (ESI):** Calculated for $C_{10}H_5BrO_4$ 267.9371 g mol^{-1}, obtained [(M+1)$^+$] 268.9426 g mol^{-1}.

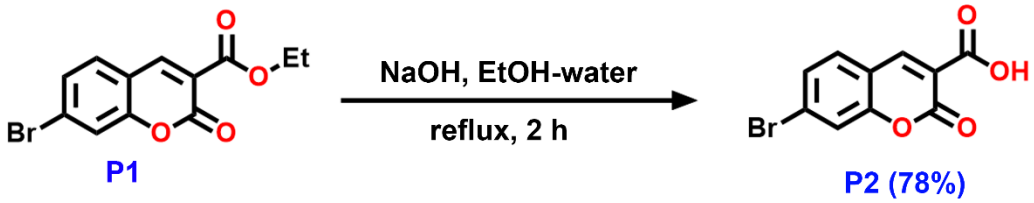

Scheme S2: Synthetic scheme of P2.

2.1.3. Synthesis of P3: To a solution of P2 (100 mg, 0.37 mmol) in dry DCM, *N*,*N*′-dicyclohexylcarbodiimide (DCC, 135 mg, 0.45 mmol), hydroxy benzotriazole (HOBt, 93 mg, 0.45

mmol), 4-dimethyl aminopyridine (DMAP, 23 mg, 0.19 mmol) and 4-(2-aminoethyl)morpholine (50 µL, 0.41 mmol) were added and stirred at room temperature (rt) for 24 h under N_2 atmosphere. The white precipitate was filtered and purified using column chromatography in silica gel ($CHCl_3$/hexane = 1:3), which resulted in P3 (yield ~ 60%).

^{1}H NMR (500 MHz, $CDCl_3$) δ: 8.95 (s, 1H), 8.26 (s, 1H), 7.52 (m, 1H), 7.40-7.34 (m, 2H), 3.77 (m, 4H), 3.21 (m, 1H), 3.09 (m, 1H), 2.78 (m, 4H), 2.63 (m, 2H). **^{13}C NMR (126 MHz, $CDCl_3$)** δ: 162.80, 156.90, 156.28, 147.76, 130.26, 128.85, 128.43, 120.18, 118.49, 116.79, 62.16, 57.43, 57.16, 53.64, 38.57, 14.15. **HRMS (ESI):** Calculated for $C_{16}H_{17}BrN_2O_4$ 380.0372 g mol^{-1}, obtained [M^+] 380.0426 g mol^{-1}.

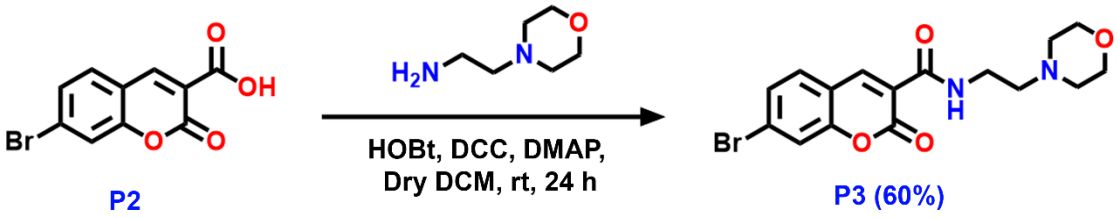

Scheme S3: Synthetic scheme of P3.

2.1.4. <u>Synthesis of DC-Luso</u>: P3 (100 mg, 0.26 mmol), diphenylamine (DPA, 58 mg, 0.34 mmol), Cs_2CO_3 (179 mg, 0.52 mmol), $Pd_2(dba)_3$ (37 mg, 0.04 mmol), and XPhos (19 mg, 0.04 mmol), toluene (10 mL) were added in a Schlenk tube and stirred at 110 °C for 24 h under an Ar atmosphere. After cooling, the organic layer was extracted with DCM (3 × 15 mL), dried using Na_2SO_4, concentrated under vacuum, and purified by column chromatography (silica gel, 15% DCM/hexane) to afford a yellow solid with a yield of 40% (48 mg, mp: 358 °C, Scheme S4).

^{1}H NMR (500 MHz, $CDCl_3$) δ 8.01 (s, 1H), 7.57 (m, 1H), 7.20 (m, 4H), 7.03 (m, 5H), 6.96 – 6.87 (m, 3H), 5.60 (s, 1H), 3.77 (m, 4H), 3.14 (m, 2H), 2.64 (m, 4H), 2.48 (m, 2H). **^{13}C NMR (126 MHz, $CDCl_3$)** δ 163.08, 156.15, 155.52, 148.05, 130.51, 129.10, 128.68, 120.43, 118.73, 117.03, 62.41, 54.12, 52.44, 37.24, 14.27. **HRMS (ESI):** Calculated for $C_{28}H_{27}N_3O_4$ 469.2002 g mol^{-1}, obtained [M^+] 469.1663 g mol^{-1}.

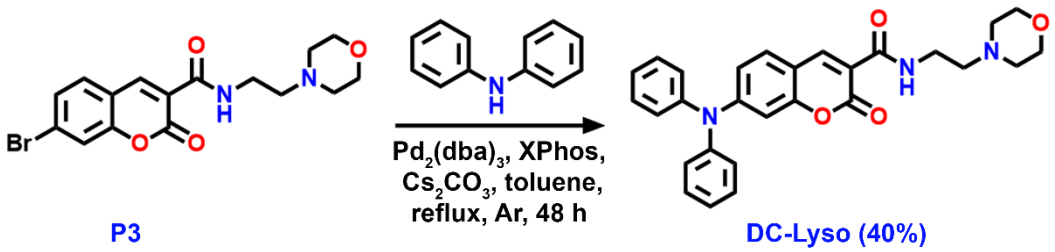

Scheme S4: Synthetic scheme of DC-Lyso.

III. Density functional theory calculations

The energy level of the frontier molecular orbitals, *i.e.*, the lowest unoccupied molecular orbitals (LUMOs) and the highest occupied molecular orbitals (HOMOs) of the respective donor (D, diphenylamine) and acceptor (A, coumarin) units, was calculated using the density functional theory (DFT) at the B3LYP/6-31G(d,p) level. Their respective electron distribution and energy values indicate the possibility of low-lying LUMO and high-energy HOMO in the resulting molecule (Fig. S1a).

The ground state optimized geometry of DC-Lyso showed a dihedral angle of ~35° around the D-A linkage (Fig. S1b). As shown in Fig. S1c, the HOMO (-5.33 eV) is predominantly localized on the donor DPA unit with a relatively small distribution over the benzene ring of the coumarin unit. However, the LUMO (-1.98 eV) is solely located on the acceptor coumarin unit. The small overlap of the HOMO-LUMO suggests the possibility of intramolecular charge transfer (ICT) characteristics in the excited state. The singlet-triplet energy gap (ΔE_{ST} = 0.21 eV in toluene, 0.18 in DMSO) of DC-Lyso was estimated through time-dependent DFT (TDDFT) calculations, which showed the possibility of temperature-assisted reverse intersystem crossing pathways (RISC, Fig. S2a). Further, the theoretical absorption spectrum of DC-Lyso was obtained using the

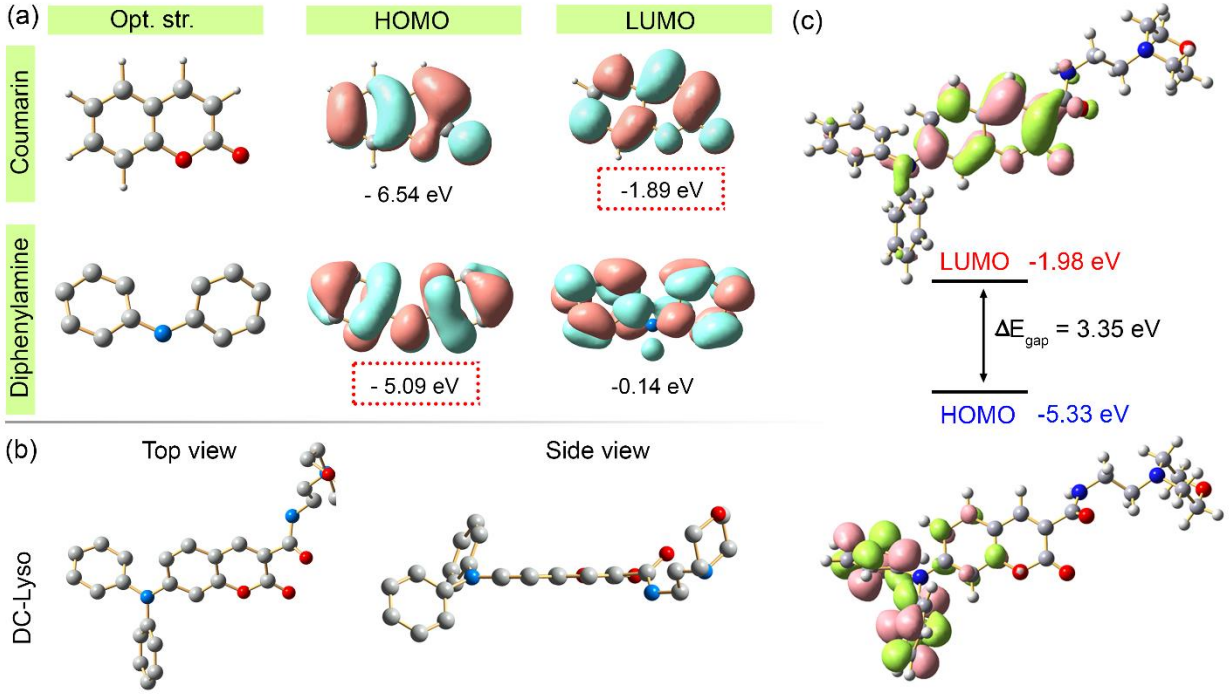

Fig. S1: (a) Ground state optimized geometry and frontier molecular orbitals of coumarin (acceptor), diphenylamine (donor), and their respective energy levels. (b) Ground state optimized geometry of DC-Lyso calculated through density functional theory (DFT) at B3LYP/6-31G(d,p) level. (c) The electron density distribution and the respective energy levels of HOMO and LUMO of DC-Lyso computed using time-dependent DFT at the B3LYP/6-31G(d,p) level.

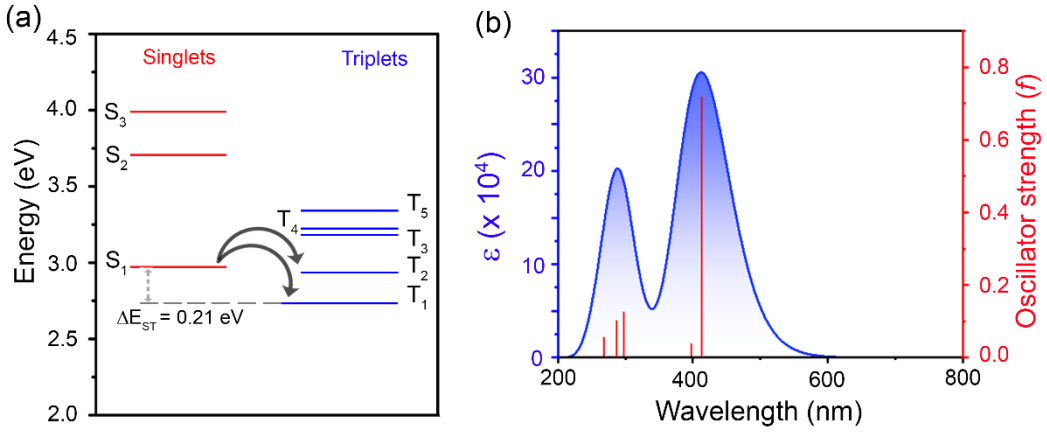

Fig. S2: (a) Schematic illustration of the energy levels of the excited singlet (S_n) and triplet (T_n) states of DC-Lyso computed through TDDFT calculations. (b) TDDFT computed absorption spectrum along with the most significant oscillator strengths (*f*) of DC-Lyso.

TDDFT calculations, indicating the possible absorption bands at ~293 nm and ~400 nm, resembling the experimental observations (Fig. S2b). The electrostatic potential calculations showed a distribution of positive surface charge over DC-Lyso (Fig. S3).

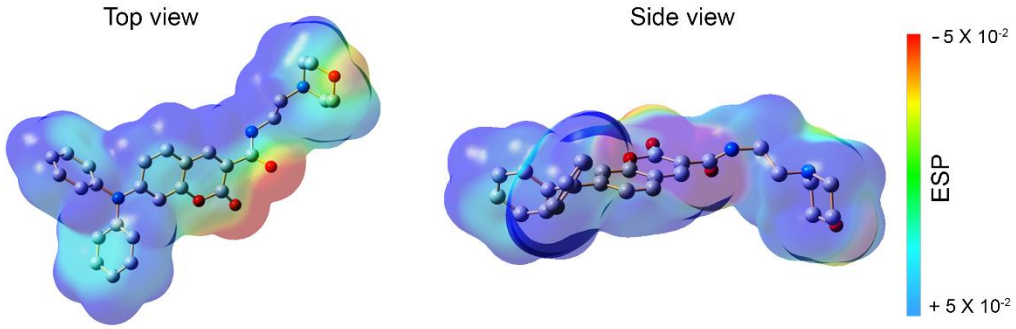

Fig. S3: Electrostatic potential (ESP) maps calculated at the B3LYP/6-31G(d,p) level depicting the higher abundance of positive surface charge.

IV. Steady-state and time-resolved spectroscopy

Absorption:

The absorption peak of DC-Lyso at ~300 nm was ascribed to the absorption of the acceptor (P3) and donor (DPA) units. The broad, red-shifted, and featureless absorption band at ~400 nm was due to the ground state intramolecular charge transfer (Fig. S4a).[10,11] The solvent-dependent absorption studies suggested the relative blue shift of the absorption maxima of DC-Lyso in high polar solvents, signifying the stabilization of the charge transfer state (Fig. S4b).[12,13]

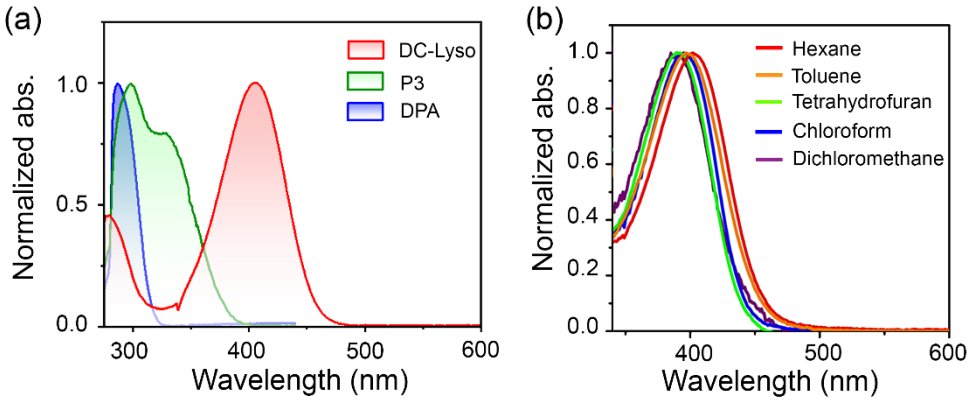

Fig. S4: Normalized absorption spectra of (a) diphenylamine (DPA), acceptor unit (P3), and DC-Lyso in toluene, and (b) DC-Lyso in organic solvents of diverse polarity.

Table S1: Molar absorption coefficient (ε) of DC-Lyso in toluene.

λ_{abs} (nm)	ε (M^{-1} cm^{-1})
293	7.44×10^4
400	9.64×10^4

Steady-state fluorescence and excited-state lifetime:

DC-Lyso showed excitation wavelength-independent emission, which signified the origin of the emission from a vertical excited state (Fig. S5a). Further, the excitation spectra were similar to the absorption spectra (Fig. S5b), demonstrating the optical purity of DC-Lyso.

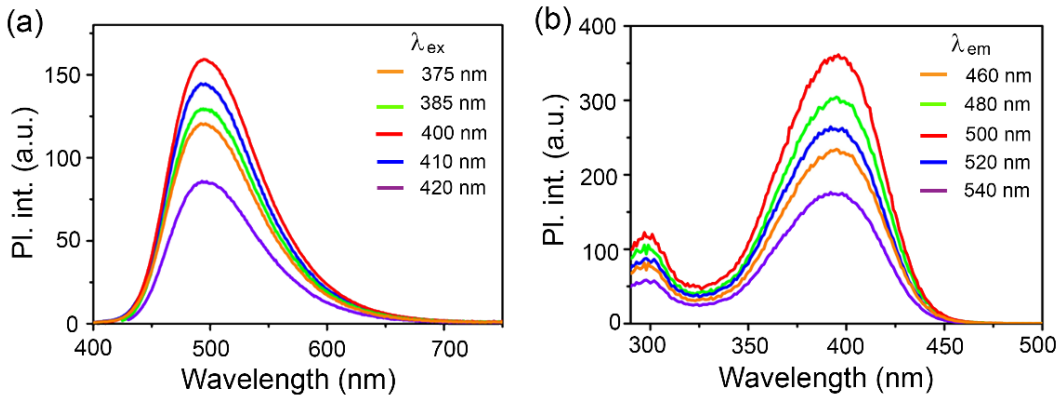

Fig. S5: (a) Emission spectra recorded at different excitation wavelengths and (b) excitation spectra monitored at different emission wavelengths of DC-Lyso in toluene.

Solvatochromism:

The Stokes shift of a fluorophore ($\Delta\bar{\nu}$) and the corresponding normalized solvent polarity parameter (E_T^N) are correlated in Reichardt's plot.[1,12,13] The mathematical equation of E_T^N is given below.

$$E_T^N = \frac{E_{T(solvent)} - E_{T(TMS)}}{E_{T(water)} - E_{T(TMS)}} \quad \text{.....(Eqn. S3)}$$

$$E_T(30) = hcN_A\nu_{max} \quad \text{.....(Eqn. S4)}$$

Where, $E_{T(solvent)}$, $E_{T(TMS)}$, and $E_{T(water)}$, represent the molar electronic transition energies in the wavenumber of a fluorophore in a specific solvent, tetramethylsilane (TMS), and water, respectively. Again, h, N_A, c, and ν_{max} refer to Planck's constant, Avogadro's number, the velocity of light in vacuum, and electronic transition energy in wavenumber, respectively.

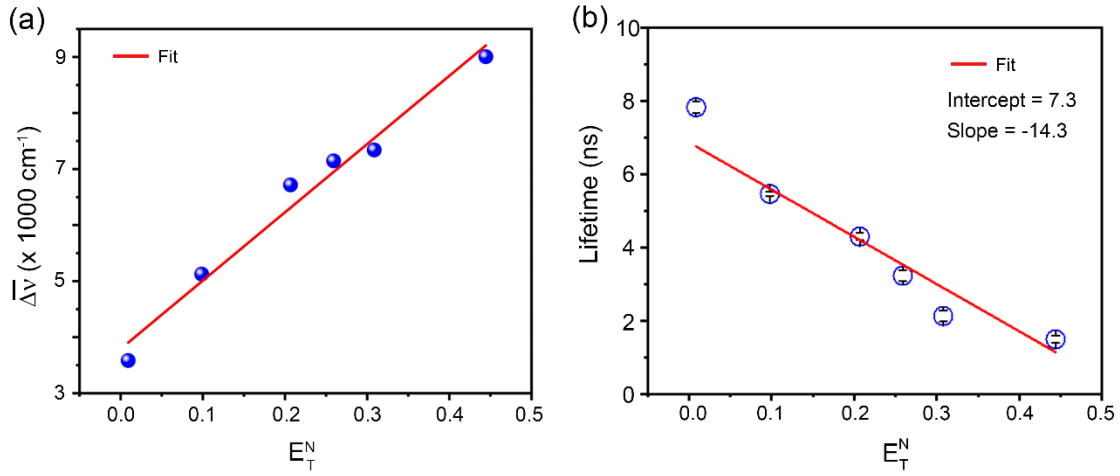

Fig. S6: The linear dependence of (a) Stokes shift ($\Delta\bar{\nu}$) and (b) average fluorescence lifetime of DC-Lyso on Reichardt's normalized solvent polarity parameter (E_T^N) for different solvents. The error bars are plotted based on three independent measurements.

Table S2: Table summarising the solvent dielectric constant (ε), Reichardt's solvent polarity ($E_T(30)$ and normalized solvent polarity (E_T^N) parameter. Absorption ($\lambda_{max(abs)}$), emission ($\lambda_{max(em)}$) maxima, full width of half maxima (FWHM), Stokes shift values in nm and cm^{-1}, quantum yield (Q.Y.) of DC-Lyso in different solvents are presented.

Entry	ε	$E_T(30)$	E_T^N	$\lambda_{max(abs)}$ (nm)	$\lambda_{max(em)}$ (nm)	FWHM (nm)	Stokes Shift (nm)	$\Delta\bar{\nu}$ (cm^{-1})	Q.Y. (%)
Hexane	1.88	31.0	0.009	395	458	67	63	25316	80 ± 2
Toluene	2.38	33.9	0.098	398	500	80	102	25125	66 ± 1
THF	7.58	37.4	0.207	400	553	107	153	25000	32 ± 1
$CHCl_3$	4.81	39.1	0.259	402	564	110	162	24876	13 ± 1
DCM	8.93	40.7	0.308	405	573	111	168	24691	9 ± 1
DMSO	46.7	45.1	0.444	406	640	127	234	24630	4 ± 1

Based on the experimental data, the lifetime of DC-Lyso can be directly converted to Reichardt's polarity parameter using a linear equation of the form,

$$E_T^N = m\tau + c \quad \text{..... (Eqn. S5)}$$

where, m = -14.3, and c = 7.3.

The nanosecond timescale decay profiles of DC-Lyso in various solvents were fitted with a bi-exponential model.[14] The increasing solvent polarity resulted in a decrease in the average decay time of DC-Lyso due to the gradual enhancement in the nonradiative transition rates (Table S3). The nonradiative (k_{nr}) and radiative (k_r) decay rates were calculated using the following equations.[1,14]

Table S3: Nanosecond timescale decay analysis compiling the decay times (τ), their contributions (α), average excited state decay time (τ_{avg}), fitting parameter (χ^2), and rates of radiative decay (k_r), and nonradiative decay (k_{nr}) of DC-Lyso in different solvents.

Solvent	$\tau_1(\alpha_1)$ (ns)	$\tau_2(\alpha_2)$ (ns)	τ_{avg} (ns)	χ^2	Q.Y. (ϕ, %)	k_r ($\times 10^7\ s^{-1}$)	k_{nr} ($\times 10^7\ s^{-1}$)
Hexane	3.3 (10)	8.5 (90)	8.1	1.09	80	10.3	2.5
Toluene	2.4 (8)	5.3 (92)	5.2	1.05	66	12.8	6.4
THF	1.7 (7)	4.5 (93)	4.3	1.13	32	7.5	15.8
$CHCl_3$	1.6 (7)	3.5 (93)	3.4	1.18	13	3.9	25.5
DCM	1.1 (6)	2.4 (94)	2.3	1.03	9	4.0	39.5
DMSO	0.8 (9)	1.8 (91)	1.7	1.01	4	2.4	56.4

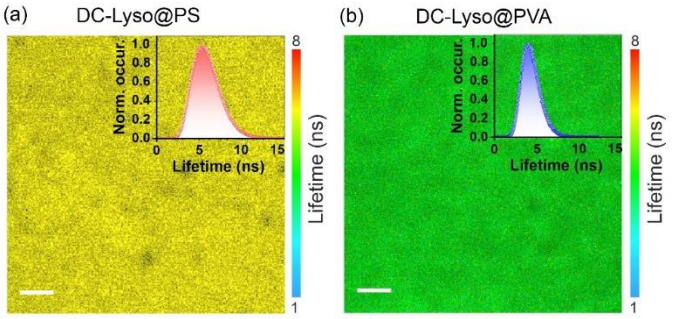

Fig. S7: Fluorescence lifetime imaging microscopy images of polymer thin films; DC-Lyso (λ_{ex} = 405 nm, λ_{em} = 425 - 800 nm), doped in (a) polystyrene (PS) and (b) polyvinyl alcohol (PVA) revealing higher polarity of PVA matrix; scale = 10 μm; inset: lifetime histograms of the corresponding thin films.

$$k_r = \frac{\phi}{\tau_{avg}} \text{ ……..(Eqn. S6)}$$

$$k_{nr} = \frac{1-\phi}{\tau_{avg}} \text{ ……..(Eqn. S7)}$$

The polarity sensing ability of DC-Lyso was further probed in polymer systems. The thin films of DC-Lyso-doped polystyrene (PS) and polyvinyl alcohol (PVA) showed distinct fluorescence lifetime variation. The lower fluorescence lifetime of PVA-doped DC-Lyso film indicates the higher polarity of PVA over the PS matrix (Fig. S7).

Microsecond timescale decay of DC-Lyso:

DC-Lyso exhibited a long-lived emission in the solution phase (Fig. S8, Table S4). The photoluminescence decay analysis revealed the presence of microsecond time decay (τ_{avg} = 0.5

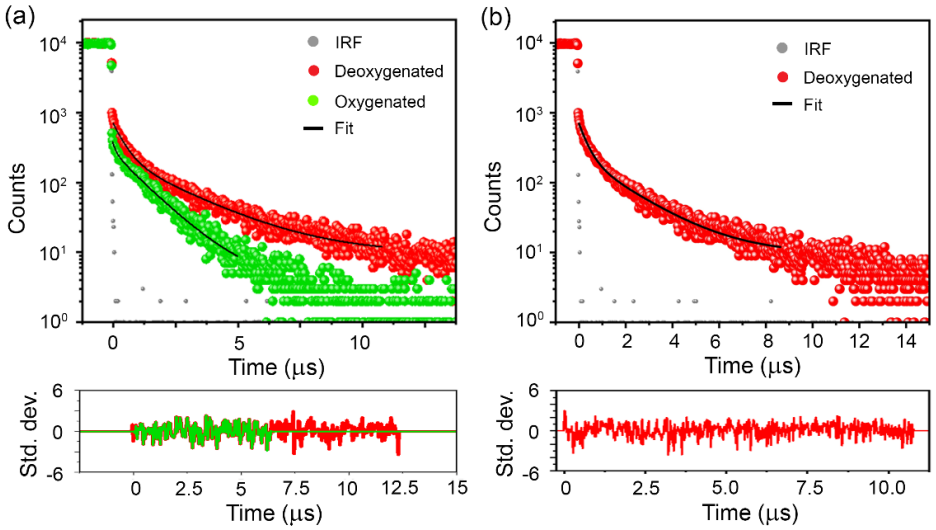

Fig. S8: Photoluminescence decay spectra of DC-Lyso in (a) dimethyl sulfoxide under oxygenated (green) and deoxygenated conditions (red, λ_{ex} = 408 nm, λ_{em} = 640 nm), and (b) toluene (λ_{ex} = 408 nm, λ_{em} = 500 nm). The corresponding residuals of the fitting range are presented.

μs) of the probe in oxygenated DMSO solution at 298 K (Fig. S8a). The long-lived emission was enhanced upon deoxygenation (τ_{avg} = 1.1 μs, Fig. S8a). DC-Lyso showed a longer average decay time (τ_{avg} = 2.0 μs) in deoxygenated toluene at 298 K (Fig. S8b).

Table S4: Microsecond timescale decay analysis of DC-Lyso compiling the decay times (τ), their contributions (α), average excited state decay time ($\tau_{avg,(DF)}$), fitting parameter (χ^2) in oxygenated (oxy) and deoxygenated (deoxy) dimethyl sulfoxide and deoxygenated (deoxy) toluene.

Sample	Time (μs)			
	τ_1 (α_1)	τ_2 (α_2)	$\tau_{avg(DF)}$	χ^2
DMSO (oxy)	0.05 (19)	0.6 (81)	0.5	1.16
DMSO (deoxy)	0.20 (42)	1.9 (58)	1.1	1.11
Toluene (deoxy)	0.70 (37)	2.8 (63)	2.0	1.11

Transient absorption spectroscopy:

The time-resolved transient difference absorption spectra analysis at different timescales indicated distinct peaks at ~400 and 500 nm of DC-Lyso in N_2-purged toluene solution upon 355 nm pulsed laser excitation (Fig. S9a). The negative peak at ~400 nm was attributed to the depleting ground states of the probe, referring to the ground state bleaching phenomenon (Fig. S9a). In contrast, the absorption band arising at 500 nm was attributed to the transient absorption of the excited states of DC-Lyso. Similar excited state absorption peaks at the nanosecond and microsecond timescale suggest the involvement of the singlet excited state for the long-lived emission (Fig. S9a).[15]

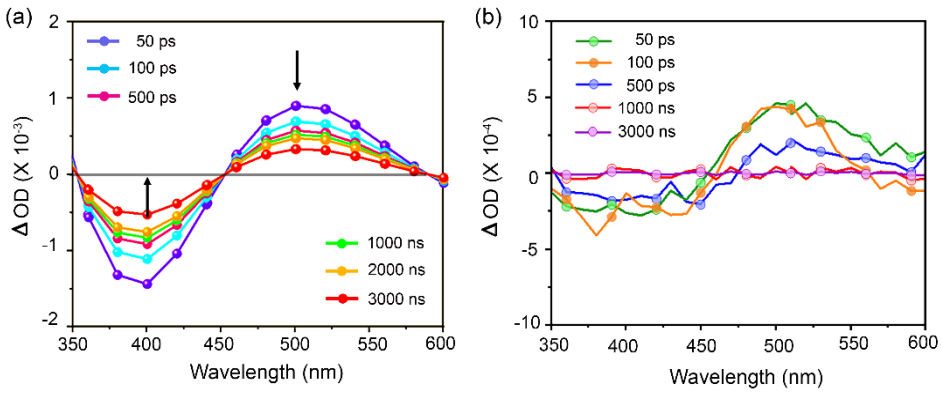

Fig. S9: Transient absorption spectra of DC-Lyso in toluene after prolonged (a) nitrogen and (b) oxygen purging depicting no emission at a longer timescale for an oxygen-purged solution, signifying the deactivation of the triplet states (λ_{ex} = 355 nm).

However, in the case of oxygenated samples, distinct peaks were observed at a lower timescale, indicating the deactivation of the long-lived emission (Fig. S9b).

Temperature-dependent emission:

The emission intensity gradually enhanced as the temperature was increased from 273 K to 333 K, a typical feature of TADF materials (Fig. S10a). The emission maxima, however, were blue shifted, probably due to the reduced polarity of the solvent at higher temperatures (Fig. S10a).[16]

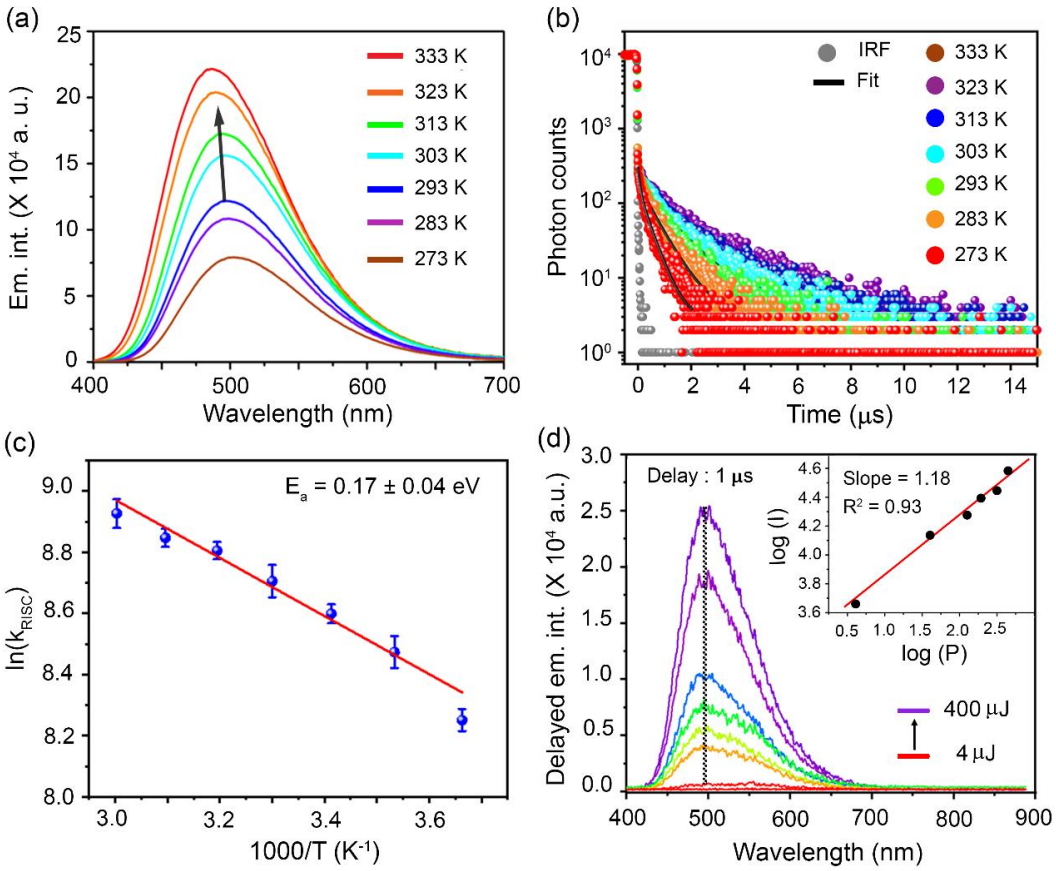

Fig. S10: (a) Emission and (b) photoluminescence decay profiles of DC-Lyso at the microsecond time-domain in deoxygenated toluene recorded at various temperatures. (c) Linear dependence of logarithmic rates of reverse intersystem crossing (RISC) with temperature. (d) The delayed emission intensity (time delay = 1 μs) variation of DC-Lyso in deoxygenated toluene under ambient conditions at different laser-power; inset: the linear dependence of the delayed emission intensity of DC-Lyso on laser-fluence, suggesting the unimolecular pathway for delayed fluorescence emission.

Activation energy for RISC:

Arrhenius model was used to calculate the activation energy associated with the RISC of DC-Lyso using the following equation,[17,18]

$$\ln(k_{RISC}) = \ln(A) - \frac{E_a}{RT} \ldots\ldots\ldots \text{(Eqn. S8)}$$

Table S5: Temperature-dependent quantum yields of prompt (ϕ_{PF}), delayed (ϕ_{DF}) fluorescence and photoluminescence (ϕ_{PL}), nanosecond timescale average decay time ($\tau_{avg(PF)}$) and microsecond timescale average decay time ($\tau_{avg(DF)}$), and subsequent rates of prompt (k_{PF}), delayed fluorescence (k_{DF}), and reverse intersystem crossing (k_{RISC}) for DC-Lyso in toluene.

Temp (K)	ϕ_{PF} (%)	ϕ_{PL} (%)	ϕ_{DF} (%)	$\tau_{avg(PF)}$ (ns)	$\tau_{avg(DF)}$ (µs)	k_{PF} (10^7 s^{-1})	k_{DF} (10^5 s^{-1})	$\phi_{PF} \times k_{PF}$ (10^5 s^{-1})	k_{RISC} (10^4 s^{-1})
273	70	75	5	5.1	0.8	19.6	12.5	13.7	2.8
283	68	77	9	5.2	0.9	19.2	11.1	13.1	4.7
293	63	78	15	5.4	1.1	18.5	9.1	11.7	5.8
303	57	86	29	5.3	2.0	18.8	5.0	10.7	5.9
313	50	86	36	5.7	2.1	17.5	4.7	8.8	6.8
323	45	84	39	5.8	2.2	17.2	4.5	7.8	7.2
333	42	85	43	6.0	2.4	16.7	4.2	7.0	7.3

Emission of DC-Lyso at low temperature:

The possibility of triplet emission of DC-Lyso was checked at 77 K (toluene, Fig. S11). The emission maximum of the toluene solution was red shifted (λ_{em} = 570 nm) at 77 K, as compared to the steady-state spectrum obtained at room temperature ($\lambda_{em,max}$ ~500 nm, Fig. 1b, Fig. S5). Photoluminescence decay analysis showed the presence of a slower component at the millisecond time domain with an average lifetime (τ_{avg}) of 181 ms (λ_{em} = 570 nm, Fig. S11a), signifying it as a phosphorescence emission. Further, time-resolved emission spectra (TRES) analysis at 298 K and 77 K was performed to reconstruct the onsets of fluorescence and phosphorescence bands, respectively, which indicated a small ΔE_{ST} of 0.21 eV (Fig. S12, Table S6), corroborating well with the temperature-dependent analysis (Fig. S10c) and theoretically obtained data (Fig. S3a).

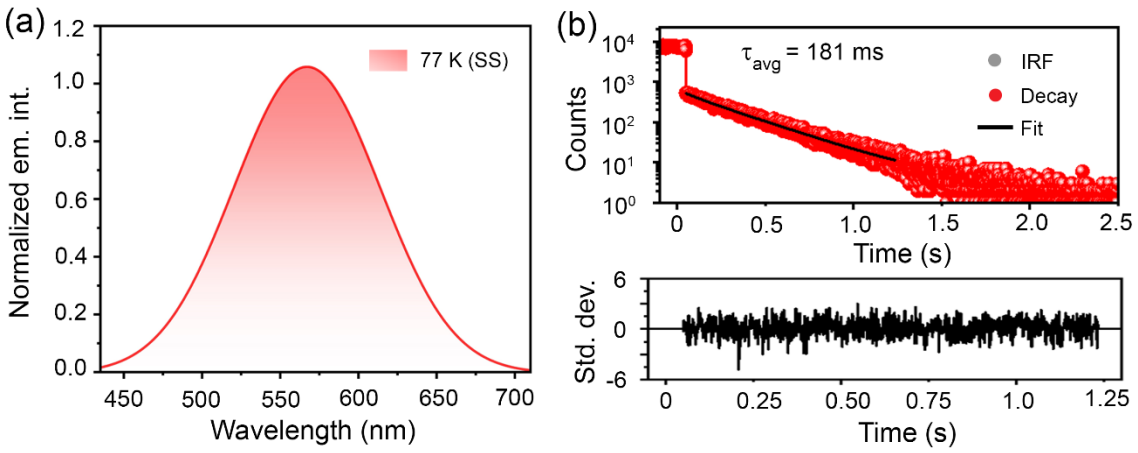

Fig. S11: (a) Normalized steady state (SS) emission spectrum and (b) the excited state decay of DC-Lyso in toluene at 77 K along with the residuals (λ_{ex} = 408 nm, λ_{em} = 570 nm).

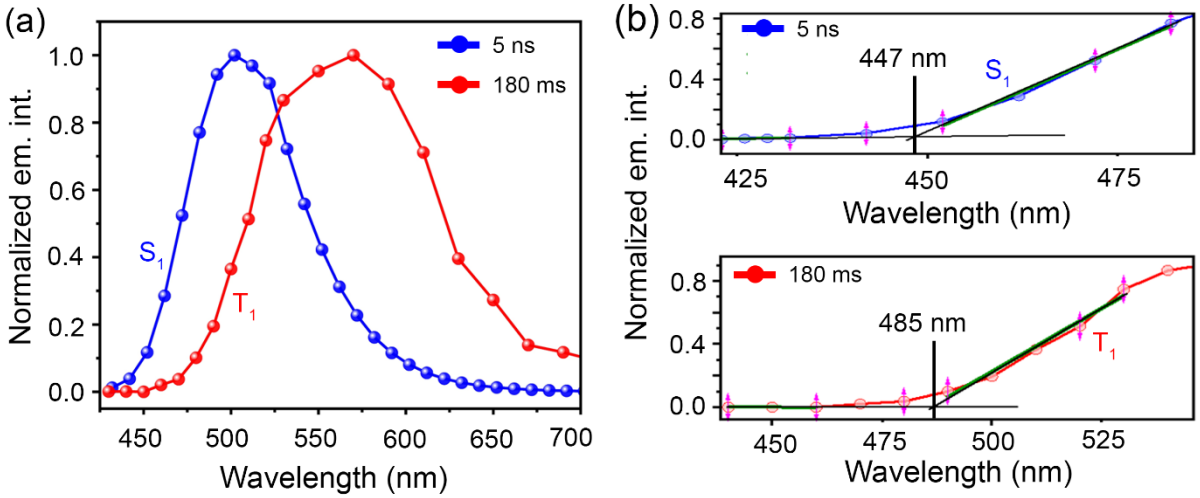

Fig. S12: (a) Normalized time-resolved emission spectra (TRES) profiles of DC-Lyso in toluene at 298 K (delay: 5 ns) and 77 K (delay: 180 ms). (b) The tangents plotted at the onset of time-gated emission profiles revealing the energy levels of the lowest energy singlet (S_1) and triplet (T_1) at 298 K and 77 K, respectively.

Table S6: The energy levels of the lowest energy singlet (S_1) and triplet (T_1) states calculated using the time-gated fluorescence and phosphorescence spectra and the singlet-triplet energy gap (ΔE_{ST}) are presented for DC-Lyso in toluene.

Compound	**S_1 (eV)**	**T_1 (eV)**	**ΔE_{ST} (eV)**
DC-Lyso	2.77	2.56	0.21

Spectroscopic properties of DC-Lyso aggregates:

The water-dispersible (90% water-DMSO) nanoaggregates of DC-Lyso, *i.e.*, DCL-NPs, exhibited similar absorption spectra to that of DC-Lyso in the solution (Fig. S13a), whereas the emission maximum of DCL-NPs centered at ~600 nm (Q.Y. ~10 ± 0.3 %, Fig. 2c). The aqueous dispersion of the nanoaggregates showed an average prompt and delayed decay times of 15 ns and 20 µs, respectively (Fig. S13b, Table S7).

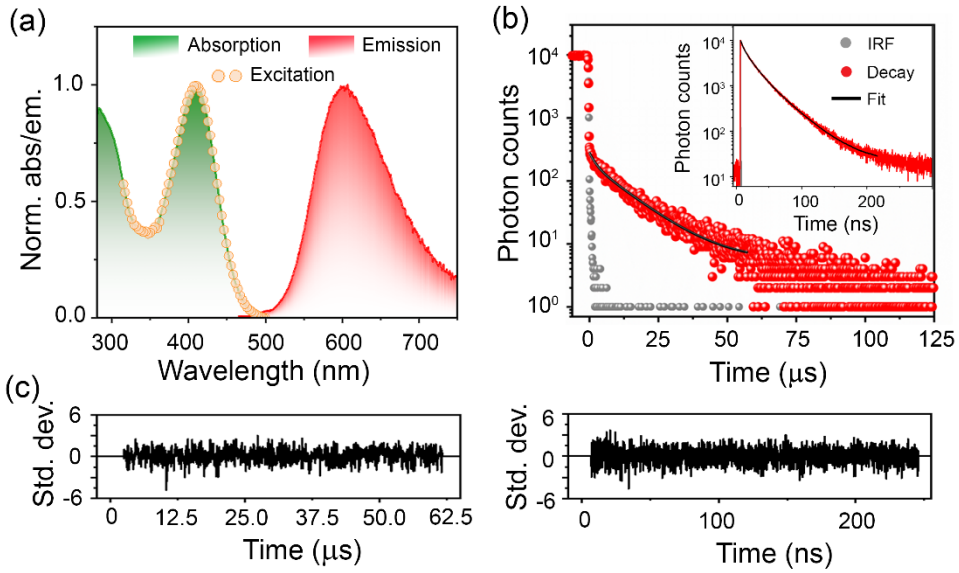

Fig. S13: (a) Normalized absorption (green), emission (red), and excitation (orange) spectra of DCL-NPs. (b) Photoluminescence decay of DCL-NPs at microsecond timescale (λ_{ex} = 461 nm, λ_{em} = 600 nm); inset: photoluminescence decay of DCL-NPs at nanosecond timescale (λ_{ex} = 470 nm, λ_{em} = 600 nm). (c) The plots of corresponding residuals of the decay fitting at the microsecond and nanosecond timescale presented in (b).

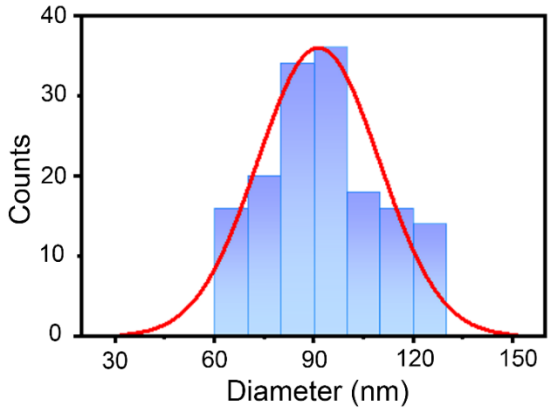

Fig. S14: Particle size distribution of DCL-NPs obtained from TEM images.

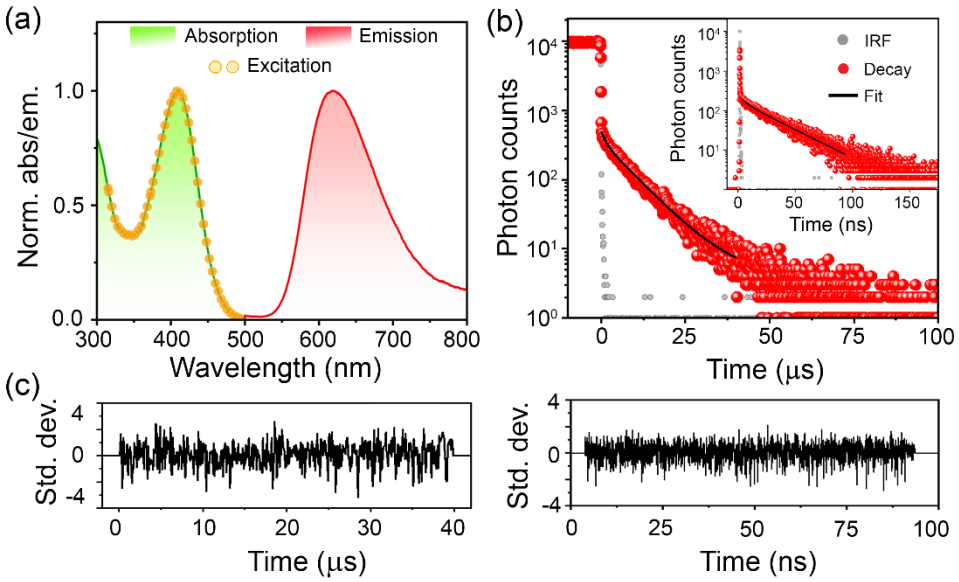

Fig. S15: (a) Normalized absorption (green), emission (red), and excitation (orange) spectra of the aqueous dispersion of DC-Lyso in water (DCL-100). (b) Photoluminescence (PL) decay of DC-Lyso dispersion at microsecond timescale (λ_{ex} = 461 nm, λ_{em} = 620 nm); inset: photoluminescence (PL) decay at nanosecond timescale (λ_{ex} = 470 nm, λ_{em} = 620 nm). (c) The plots of corresponding residuals of the decay fitting at the microsecond and nanosecond timescale presented in (b).

The dispersion in water (DCL-100) was prepared by injecting 6 μL of 1 mM DMSO solution of DC-Lyso into 3 mL of MilliQ water (resistivity = 18.2 MΩ cm) under sonication for 1 min. The aqueous dispersion of DC-Lyso (DCL-100) exhibited an absorption peak around ~400 nm, while the emission maximum was centered at ~620 nm (Q.Y. ~6 %). The aqueous dispersion showed an average prompt and delayed decay times of 11 ns and 10 μs, respectively (Fig. S15, Table S8). TEM images revealed a spherical morphology with a larger particle diameter (~200 nm) with broad heterogeneity (Fig. S16). The dispersion obtained in 90% water and 10% DMSO (average particle diameter ~90 ± 20 nm) was used for the imaging studies due to its higher quantum yield (10%) and average decay time (prompt: 15 ns, delayed: 20 μs, Table S7).

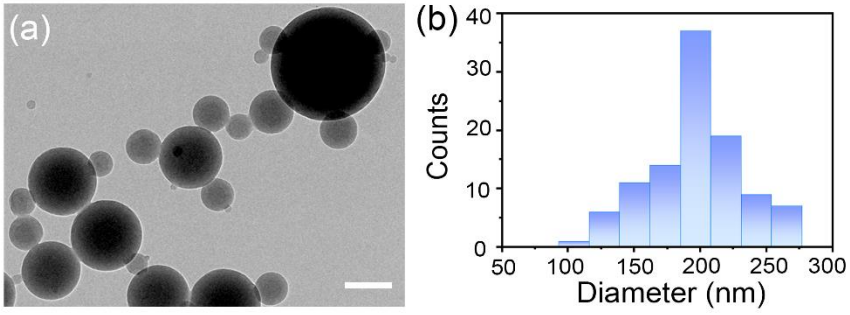

Fig. S16: (a) High-resolution transmission electron microscopy (HRTEM) image of the aqueous dispersion of DC-Lyso (DCL-100), scale = 200 nm. (b) Particle size distribution of the aqueous dispersion of DC-Lyso obtained from TEM images.

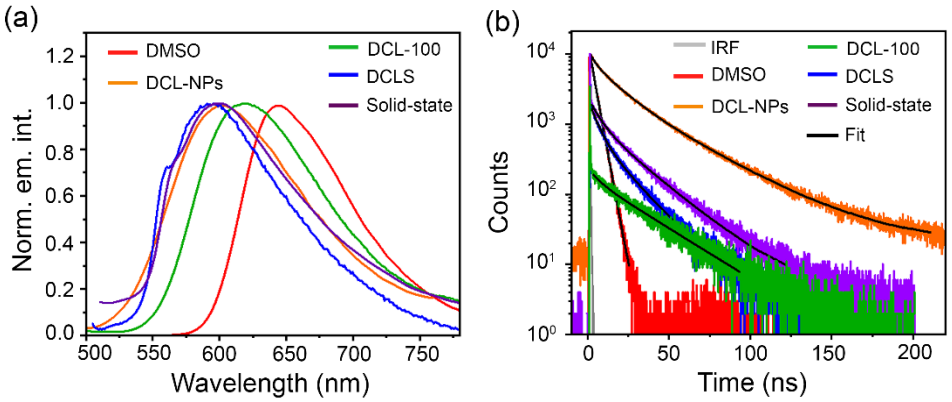

Fig. S17: (a) Normalized emission profiles of DC-Lyso in DMSO (red), DC-Lyso nanoparticles (DCL-NPs, dispersion in 90% water and 10% DMSO, orange), DCL-100 (dispersion in pure water, green), solid dispersed in water (DCLS, blue), and solid-state (purple). (b) Corresponding decay profiles at the nanosecond timescale.

Table S7: Nanosecond and microsecond timescale decay analysis of DCL-NPs compiling the decay times (τ), their contributions (α), average excited state decay time (τ_{avg}), fitting parameter (χ^2) in water.

Entry	τ_1 (α_1)	τ_2 (α_2)	τ_{avg}	χ^2
Prompt fluo. (ns)	20.1 (63)	7.2 (37)	15.3	1.01
Delayed fluo. (µs)	22.0 (84)	9.6 (16)	20.0	1.03

Table S8: Nanosecond and microsecond timescale decay analysis of DCL-100 compiling the decay times (τ), their contributions (α), average excited state decay time (τ_{avg}), fitting parameter (χ^2) in water.

Entry	τ_1 (α_1)	τ_2 (α_2)	τ_{avg}	χ^2
Prompt fluo. (ns)	15.3 (65)	4.2 (35)	11.4	1.05
Delayed fluo. (µs)	12.0 (77)	3.7 (23)	10.1	1.08

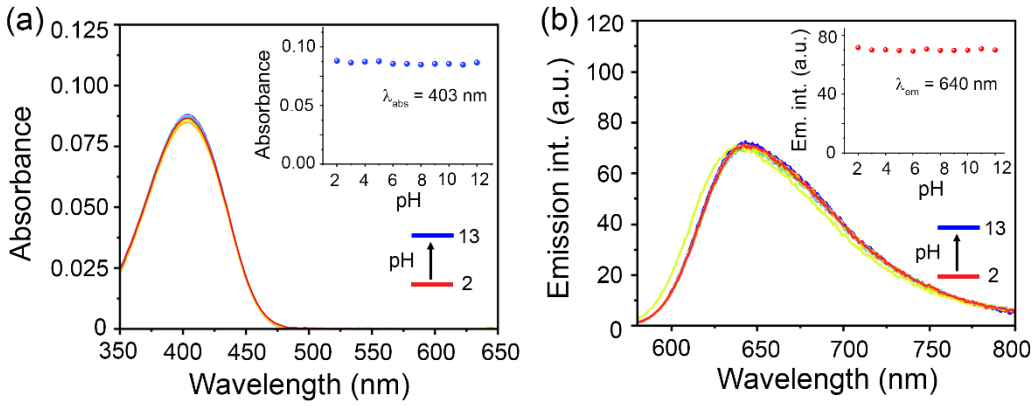

Fig. S18: pH-independent (a) absorption and (b) emission profiles of DC-Lyso in aqueous pH buffer (5% DMSO); inset: the absorbance at 403 nm, emission intensity at 640 nm, for Fig. S18 (a, b) at different pH.

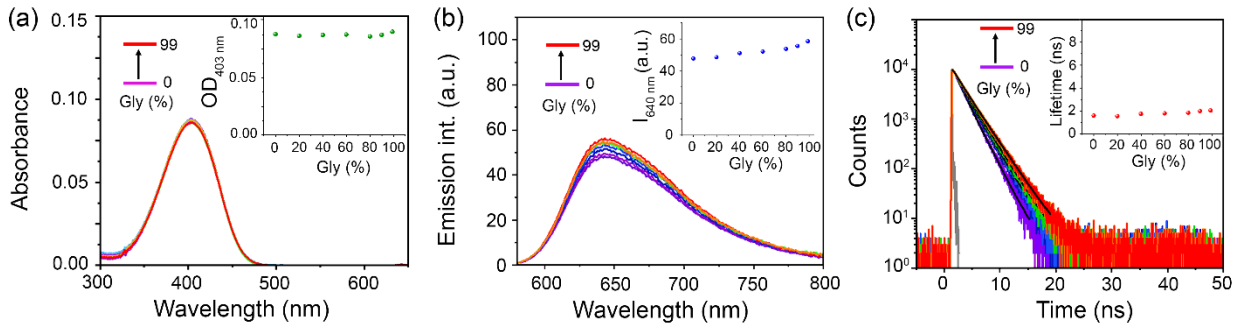

Fig. S19: (a) Absorption, (b) emission, and (c) fluorescence decay profiles of DC-Lyso in MeOH-glycerol binary solvent mixture; inset: the absorbance at 403 nm, emission intensity at 640 nm, and average fluorescence lifetime with increasing glycerol percentages for Fig. S19 (a - c). A viscosity-independent spectral behavior is observed.

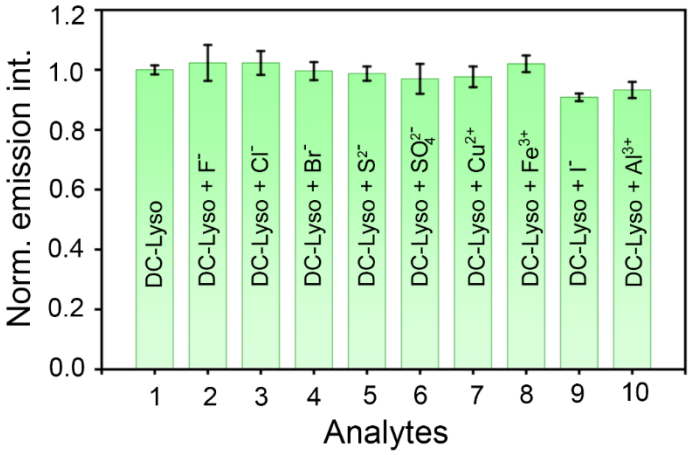

Fig. S20: Variation of emission intensity of DC-Lyso in the presence of different biologically relevant analytes; the error bars are represented based on three independent measurements (n = 3).

V. Cell viability

MTT assay:

The cytotoxicity of DC-Lyso and its aqueous dispersion of nanoparticles, DCL-NPs, was evaluated using MTT assay in HeLa cells. The probes showed high cell viability (~90 %) even at a high incubation concentration for 24 h (Fig. S21a, b). The probe showed high cell viability (~80 ± 5 %) at a working concentration of 2 μM after 5 days of incubation (Fig. S21c).

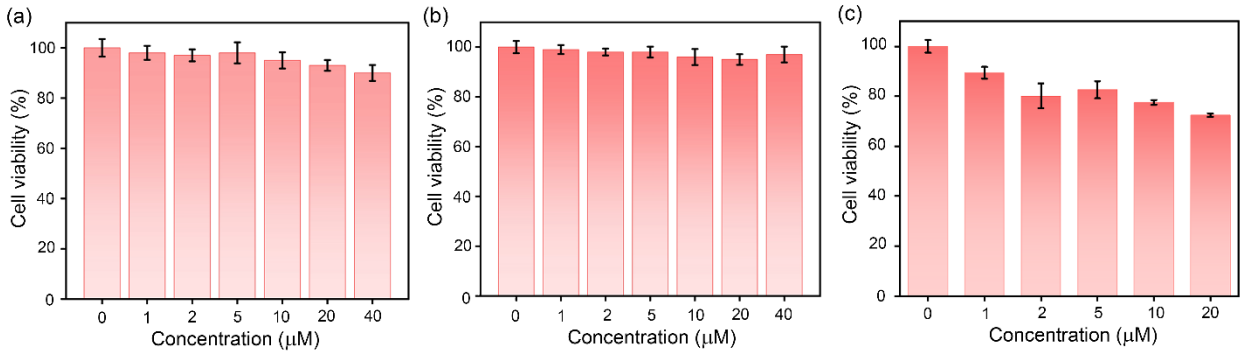

Fig. S21: MTT assay signifies the high cell viability of HeLa cells incubated with (a) DC-Lyso solution and (b) aqueous dispersion of DCL-NPs for 24 h, and (c) different concentrations of DC-Lyso solution for 5 days; the error bars are represented based on triplicate measurements (n = 3).

JC-1 assay:

The FACS data revealed the presence of ~83% of healthy HeLa cells based on mitochondrial membrane potential as determined by JC-1 assay even at a high concentration of DC-Lyso (10 μM) for 24 h incubation (Fig. S22). At a working concentration of 2 μM (used for imaging), ~87% of healthy cells were observed, demonstrating the good cytocompatible nature of DC-Lyso (Fig. S22).

Phototoxicity assay of DC-Lyso:

The phototoxicity of DC-Lyso under 405 nm laser irradiation was checked using the SYBR Green I-propidium iodide assay in HeLa cells (Fig. S23). SYBR Green I is known for only staining the nuclei of live cells, whereas propidium iodide only stains the nuclei of dead cells. The cells were first treated with DC-Lyso and then irradiated under a 405 nm laser for different time intervals. Thereafter, the cells were co-incubated with SYBR Green (500 nM) and propidium iodide (500 nM) and washed thrice with PBS. The images taken at the respective green and red channels indicate the low phototoxicity effect of DC-Lyso under laser irradiation (Fig. S23).

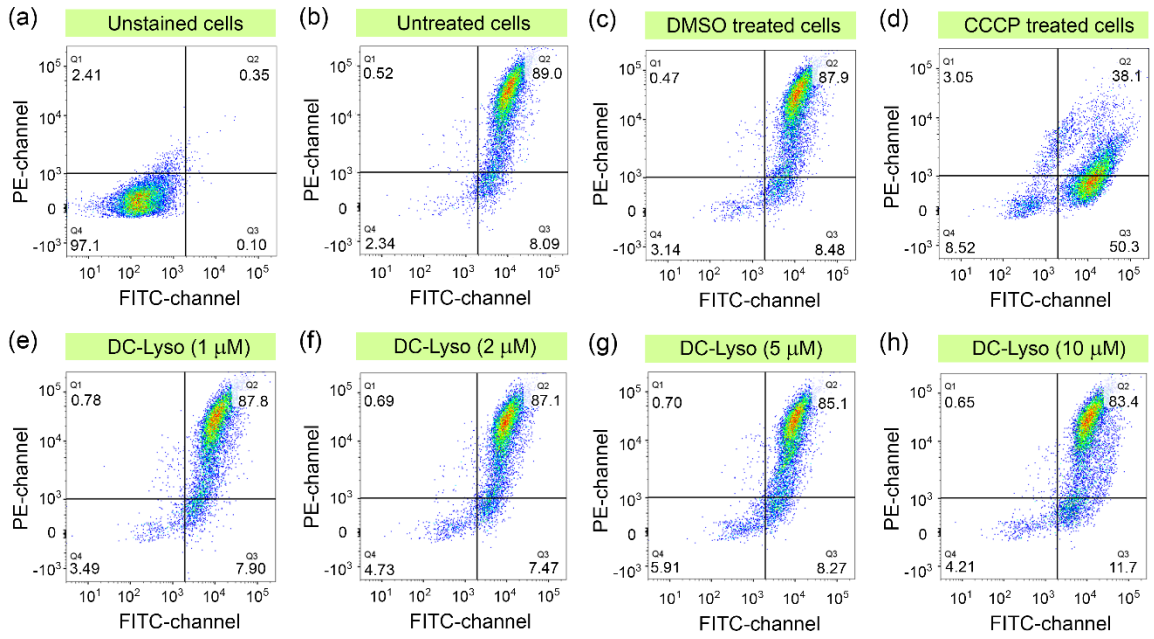

Fig. S22: Quantification of the mitochondrial membrane potential of HeLa cells using fluorescence activated single-cell sorting (FACS). Top panel: FACS data of (a) unstained cells, *i.e.*, cells without DMSO, DC-Lyso, and JC-1 treatment, (b) untreated cells, *i.e.*, cells treated with JC-1 but not with DMSO and DC-Lyso, (iii) DMSO treated, and (iv) carbonyl cyanide *m*-chlorophenyl hydrazone (CCCP, 50 μM). Bottom-panel: FACS data of HeLa cells treated with JC-1 (2 μM) and incubated with DC-Lyso at different concentrations for 24 h; (e) 1 μM, (f) 2 μM (g) 5 μM, and (h) 10 μM. The emission was recorded in the green (FITC) channel for JC-1 monomer (λ_{ex} = 488 nm, λ_{em} = 510 - 550 nm) and red (PE) channel for JC-1 aggregates (λ_{ex} = 488 nm, λ_{em} = 580 - 600 nm), respectively.

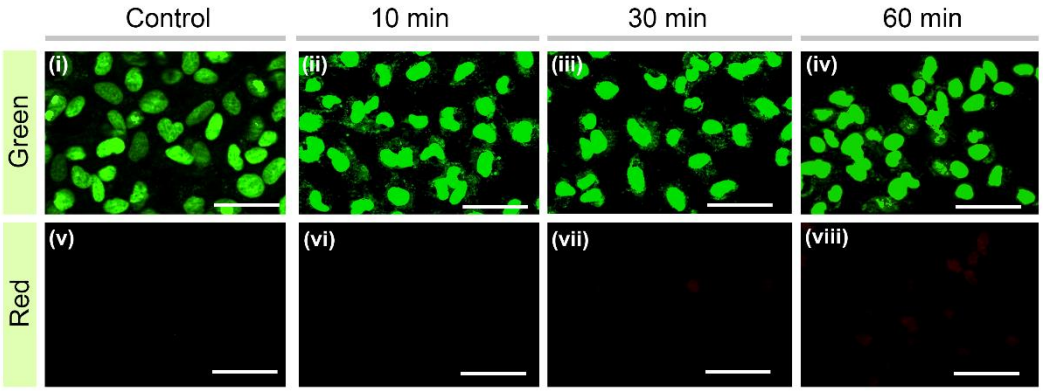

Fig. S23: SYBR Green I (dye for live cell staining, λ_{ex} = 450 - 490 nm, λ_{em} = 500 - 550 nm) and propidium iodide (dye for dead cell staining, λ_{ex} = 538 - 562 nm, λ_{em} = 570 - 640 nm) assay for the determination of the phototoxicity of DC-Lyso under 405 nm laser (laser power ~100 mW, power density: 20 mW cm^{-2}) irradiation in HeLa cells; (i, v) control set with no external laser irradiation, laser irradiation for (ii, vi) 10 min, (iii, vii) 30 min, (iv, viii) 60 min irradiation; scale = 50 μm. The abundance of a higher number of nuclei stained in the green channel than in the red channel reveals the low phototoxicity effect of DC-Lyso.

VI. Intracellular imaging

Time-dependent incubation:

DC-Lyso exhibited fast cellular internalization in live cells (Fig. S24). Bright fluorescence signals were observed from HeLa cells incubated with the probe only for 1 - 10 min at 37 °C under a 5% CO_2 atmosphere. The fast staining ability of DC-Lyso was attributed to the positive surface charge (Fig. S3), which could be beneficial for faster membrane permeabilization.[19]

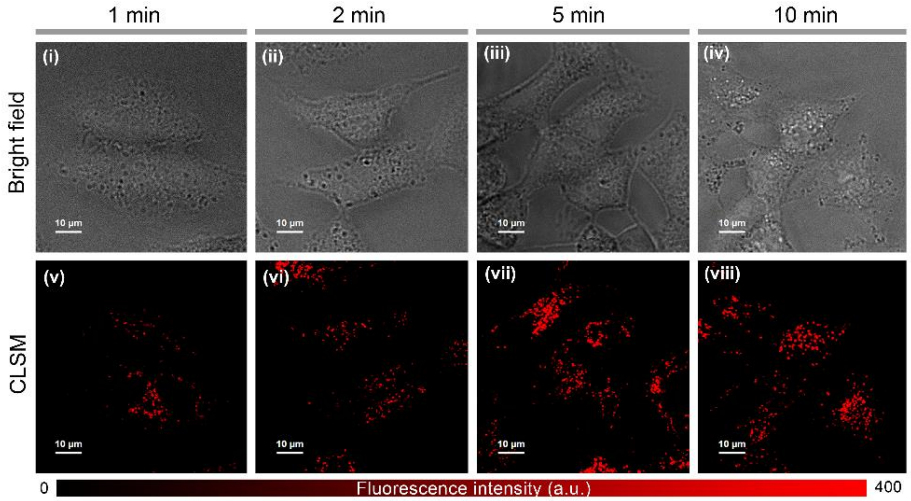

Fig. S24: Colocalization study using confocal laser scanning microscopy (CLSM) of HeLa cells incubated with DC-Lyso for different time periods; (i, ii, iii, iv) bright field images, (v, vi, vii, viii) fluorescence images (λ_{ex} = 405 nm, λ_{em} = 620 - 660 nm); scale = 10 μm. The intracellular intensity scale of DC-Lyso is also presented.

Mechanism of intracellular internalization:

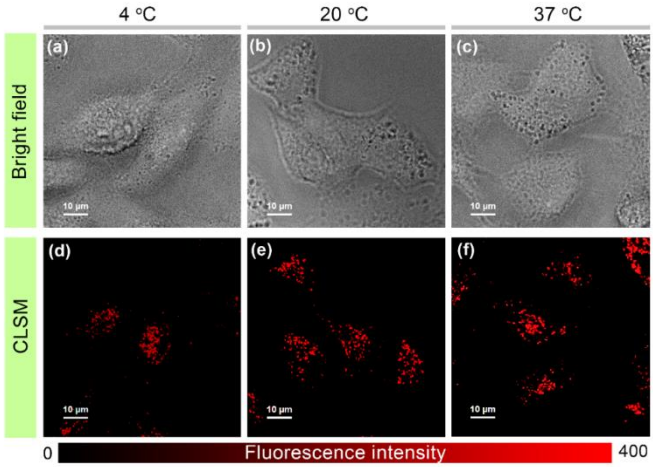

Fig. S25: Confocal laser scanning microscopy (CLSM) images of DC-Lyso in HeLa cells incubated at different temperatures (a, d) 4 °C, (b, e) 20 °C, and (c, f) 37 °C; (a - c) bright field images, (d - f) fluorescence images (λ_{ex} = 405 nm, λ_{em} = 488 - 800 nm); scale = 10 µm.

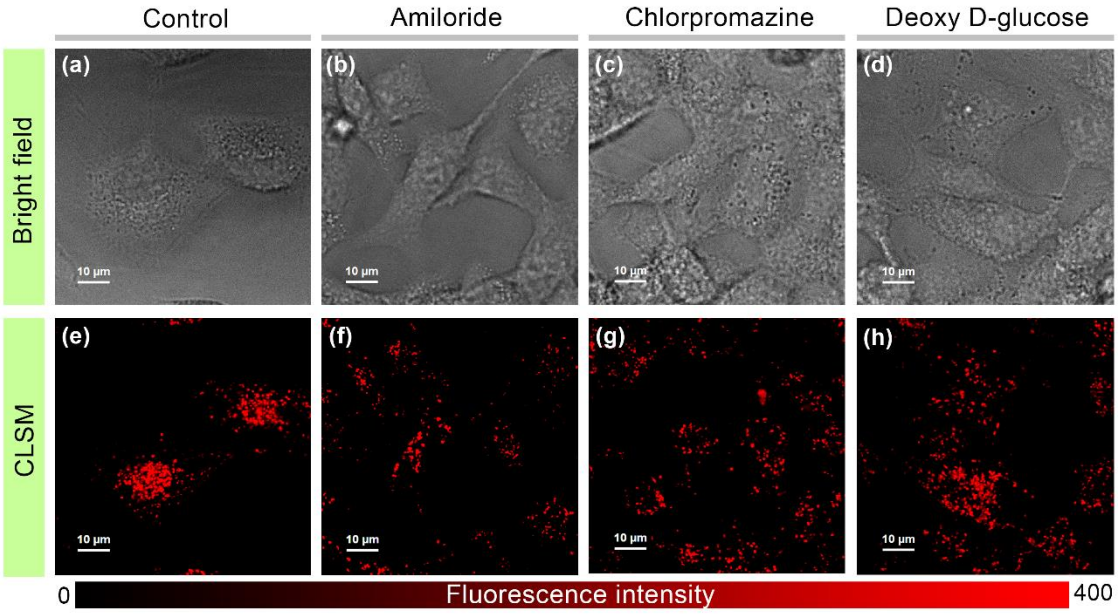

Fig. S26: Confocal laser scanning microscopy (CLSM) images of DC-Lyso stained HeLa cells incubated with (a, e) complete growth media, considered as control, (b, f) amiloride, (c, g) chlorpromazine, and (d, h) deoxy D-glucose indicating similar intracellular fluorescence intensities; (a - d) bright field images, (e - h) fluorescence images (λ_{ex} = 405 nm, λ_{em} = 488 - 800 nm); scale = 10 µm.

Colocalization studies:

The specific lysosome targeting ability of DC-Lyso was further checked by colocalization studies in HeLa cells using commercial organelle tracking dyes like LysoTracker™ Green (LTG, lysosome), DAPI (nucleus), CellMask™ Green (CMG, cell membrane), and MitoTracker™ Green (MTG, mitochondria). DC-Lyso and tracker dye costained cells displayed high Pearson's correlation coefficient only for LTG, indicating the specific lysosome targeting ability of DC-Lyso (Fig. S27, Fig. S28).

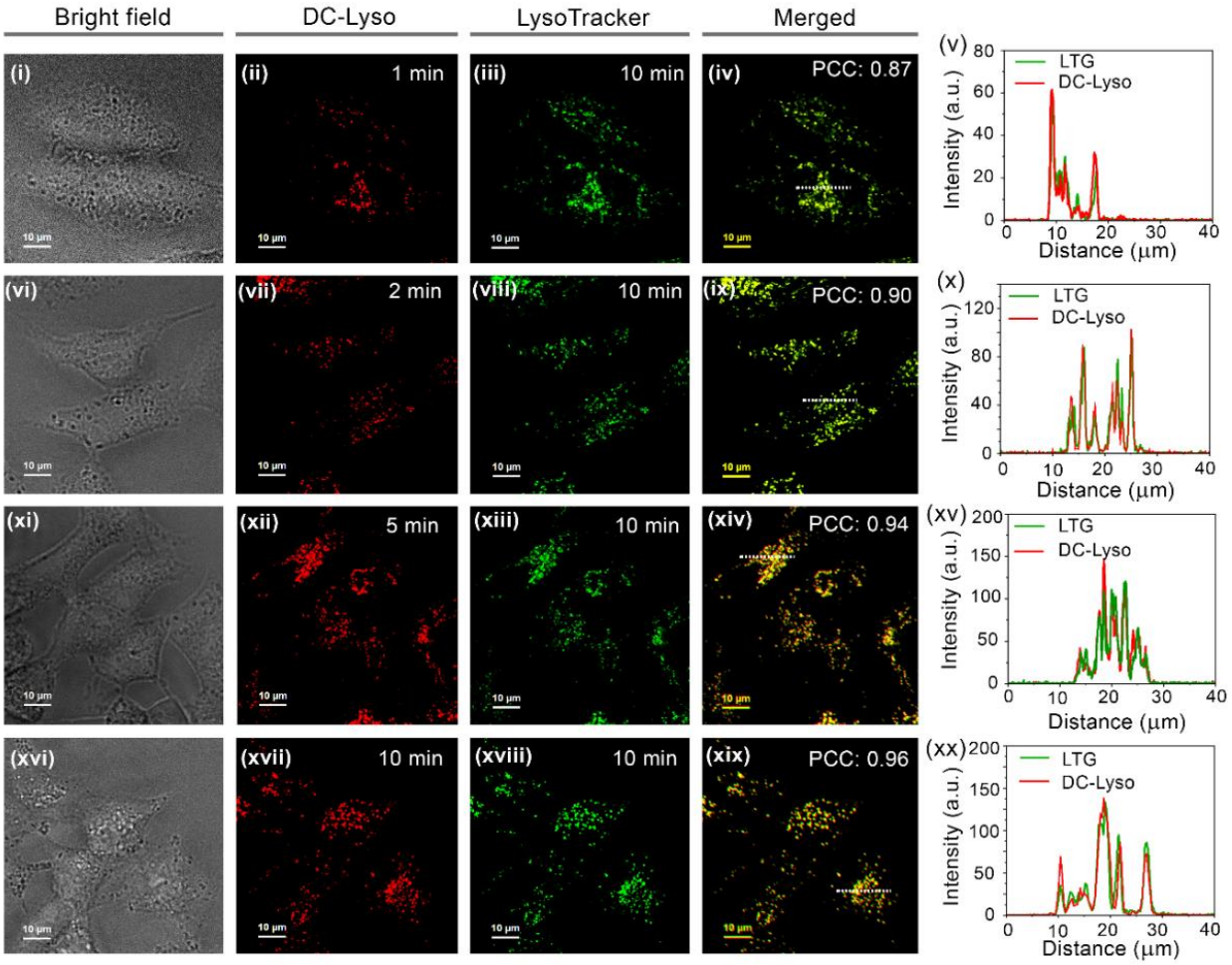

Fig. S27: Colocalization study using confocal laser scanning microscopy (CLSM) of HeLa cells coincubated with DC-Lyso and LysoTracker™ Green (LTG); (i, vi, xi, xvi) bright field images, cells incubated with (ii, vii, xii, xvii) DC-Lyso (λ_{ex} = 405 nm, λ_{em} = 620 - 660 nm), (iii, viii, xiii, xviii) LTG (λ_{ex} = 470 nm, λ_{em} = 520 - 540 nm), and (iv, ix, xiv, xix) corresponding merged images of DC-Lyso and LTG channels; Pearson's coefficient of colocalization (PCC) values are indicated for DC-Lyso incubation time: 1, 2, 5, and 10 min: scale = 10 μm. (v, x, xv, xx) Intracellular intensity profiles of DC-Lyso and LTG for the dotted white line depicted, respectively, in the images (iv, ix, xiv, xix) ascertaining colocalization of DC-Lyso with LTG in live cells.

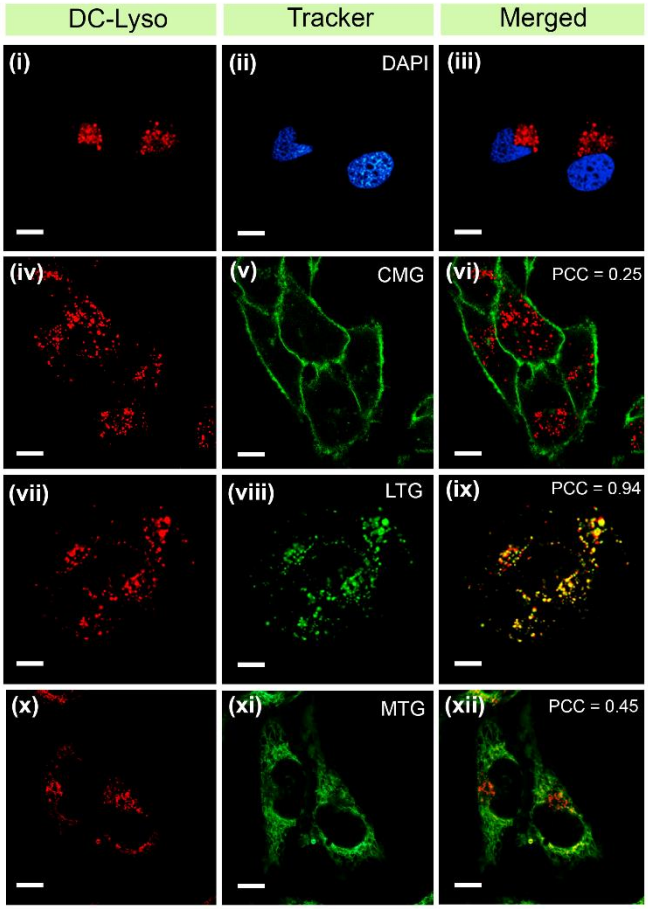

Fig. S28: CLSM colocalization studies of HeLa cells coincubated with DC-Lyso (λ_{ex} = 405 nm, λ_{em} = 620 - 660 nm) and commercially available organelle tracker dyes; HeLa cells stained with (i, iv, vii, x) DC-Lyso, (ii) 4',6-diamidino-2-phenylindole (DAPI, λ_{ex} = 405 nm, λ_{em}= 400 – 445 nm), (v) CellMask^{TM} Green (CMG), (viii) LysoTracker^{TM} Green (LTG), and (xi) MitoTracker^{TM} Green (MTG). The merged images of (iii) i and ii, (vi) iv and v, (ix) vii and viii, and (xii) x and xi, depict a high Pearson's coefficient of colocalization (PCC) value of 0.94 only for DC-Lyso with LTG, indicating lysosome targeting ability of the probe; scale = 10 μm. For green channel images (v, viii, xi) λ_{ex} = 470 nm, λ_{em} = 500 - 540 nm.

Z-scan imaging:

DC-Lyso was employed for the visualization of the 3D distribution of lysosomes in live cells. CLSM imaging at different heights of the cell showed the varied distribution of lysosomes along the z-axis (Fig. S29).

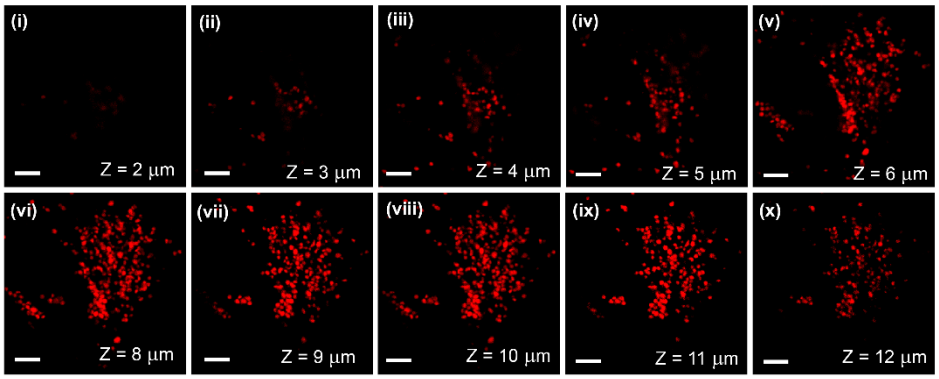

Fig. S29: Z-scan images of HeLa cells stained with DC-Lyso (λ_{ex} = 405 nm, λ_{em} = 425 - 800 nm) at different heights of the cell with respect to the focal plane (Z = 0 μm); scale = 10 μm.

Intracellular photostability:

The intracellular photostability of DC-Lyso was checked under continuous laser irradiation of constant power (laser power = 0.6 μW, power density = 0.12 μW cm^{-2}, Fig. S30). DC-Lyso stained HeLa cells under continuous laser irradiation for 2 h indicated a marginal loss of intensity, suggesting excellent photostability of DC-Lyso (Fig. S30**)**. The mean fluorescence intensity (MFI) obtained from the images also supported the observations (Fig. S30). Normalizing the initial fluorescence intensity of the probes, the calculated percentage of intensity showed ~88% signal retention for DC-Lyso (Fig. S30), demonstrating high photostability.

The intracellular photostability of DC-Lyso was compared with commercial lysosome-specific probes like LysoTracker™ Green (LTG) and LysoTracker™ Red (LTR) under continuous laser irradiation of constant power (laser power = 10 μW, power density = 2 μW cm^{-2}, Fig. S31) for 30 min. Normalizing the initial fluorescence intensity of the probes, the calculated percentage of intensity loss was ~50% for LTG, whereas only 15% signal loss was observable for DC-Lyso (Fig. S31).

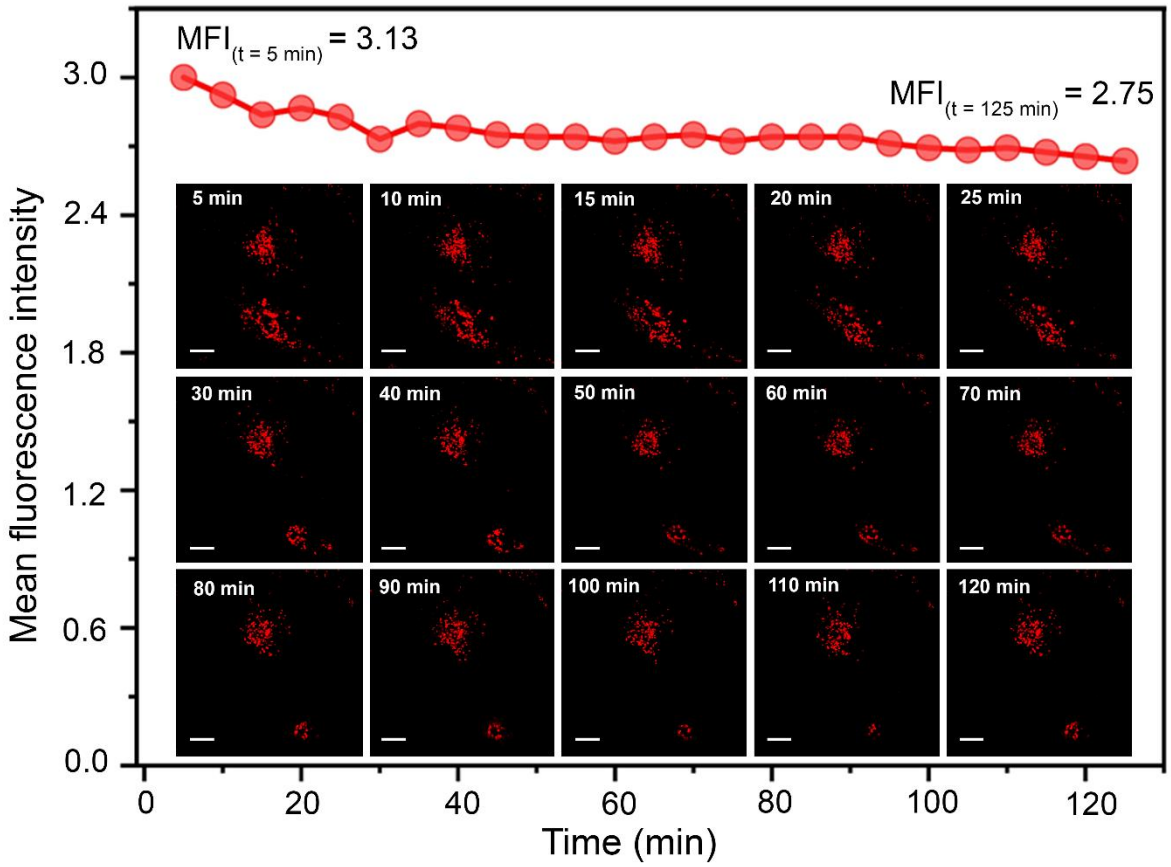

Fig. S30: Intracellular photostability of DC-Lyso; time-dependent mean fluorescence intensity (MFI) variation of DC-Lyso (2 μM) stained HeLa cells for 125 min under continuous laser irradiation (λ_{ex} = 405 nm, λ_{em} = 488 - 800 nm, laser power = 0.6 μW, power density = 0.12 μW cm^{-2}) showing superior photostability of DC-Lyso; scale = 10 μm.

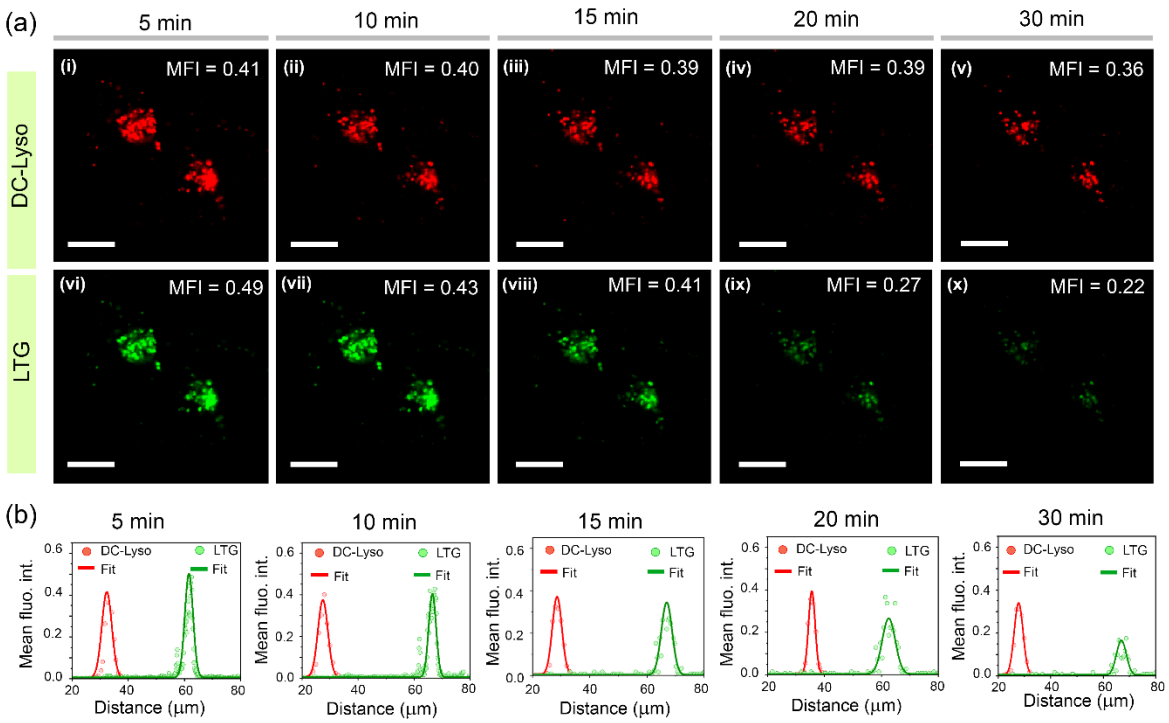

Fig. S31: (a) Comparative intracellular photostability of DC-Lyso and commercially available lysosome tracker dye in HeLa cells; images of cells stained with (i - v) DC-Lyso (λ_{ex} = 405 nm, λ_{em} = 620 - 660 nm) and (vi - x) LysoTracker^{TM} Green, (LTG, λ_{ex} = 470 nm, λ_{em} = 525 - 560 nm), for 30 min under continuous laser irradiation (laser power = 10 μW, power density = 2 μW cm^{-2}) indicating superior photostability of DC-Lyso; scale = 10 μm. (b) The comparative intracellular mean fluorescence intensity plots of DC-Lyso (red) and LTG (green).

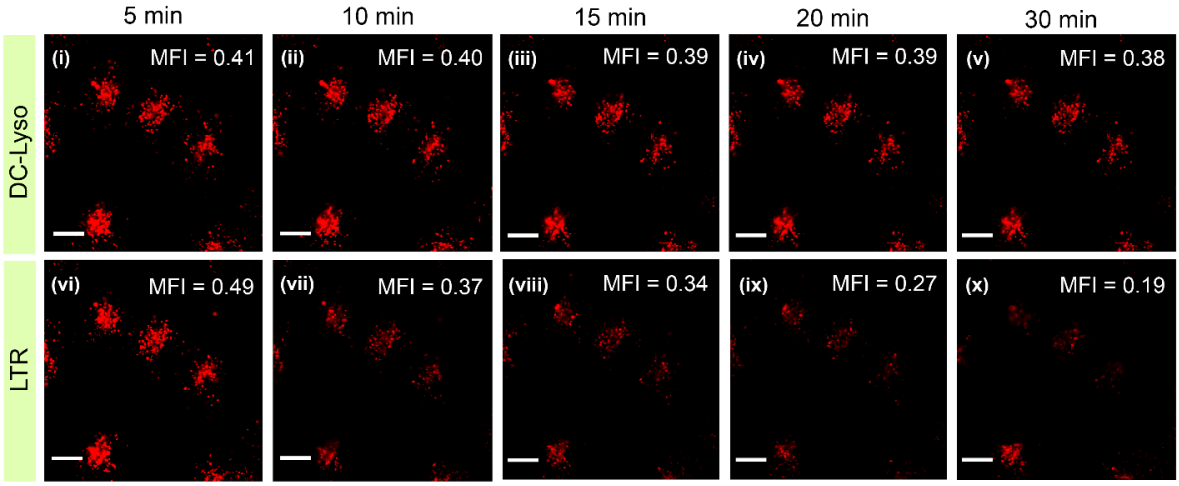

Fig. S32: Comparative intracellular photostability of DC-Lyso and commercially available lysosome tracker dye in HeLa cells; images of cells stained with (i - v) DC-Lyso (λ_{ex} = 405 nm, λ_{em} = 620 – 660 nm) and (vi - x) LysoTracker^{TM} Red, (LTR, λ_{ex} = 530 nm, λ_{em} = 620 – 660 nm), for 30 min under continuous laser irradiation (laser power = 10 μW, power density = 2 μW cm^{-2}) demonstrating superior photostability of DC-Lyso; scale = 10 μm. The comparative intracellular mean fluorescence intensity values of DC-Lyso and LTR over the duration of the experiment are also indicated.

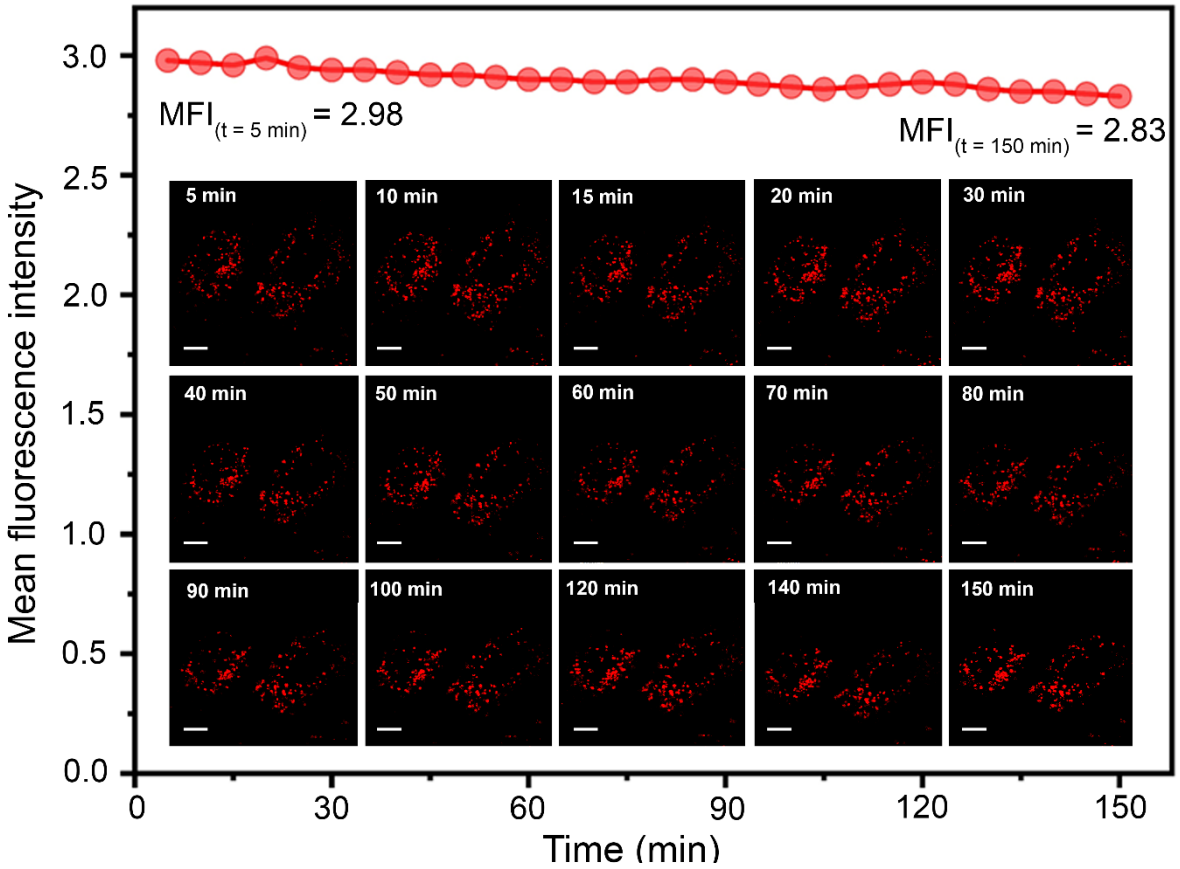

Fig. S33: Intracellular photostability of DC-Lyso nanoparticles (DCL-NPs, 2 μM) stained HeLa cells for 150 min under continuous laser irradiation (λ_{ex} = 470 nm, λ_{em} = 488 - 800 nm, laser power = 1 μW, power density = 0.2 μW cm^{-2}) demonstrating high photostability of DCL-NPs; scale = 10 μm. The mean fluorescence intensities (MFIs) over the duration of the experiment are also indicated.

Similarly, the photostability comparison for DC-Lyso and LTR revealed ~55% intensity loss for LTR (Fig. S32). The high photostability of DC-Lyso could be beneficial for tracking lysosomal motions and interorganelle interactions for longer time periods.

The aqueous dispersion of DC-Lyso in 90% water, *i.e.*, DCL-NPs, indicated higher intracellular photostability up to 150 min of continuous laser irradiation, with no significant intensity loss. The mean fluorescence intensity plots depicted ~94% retention of the original intensity over time (150 min, Fig. S33).

Fluorescence lifetime imaging microscopy (FLIM):

The FLIM images of live HeLa cells demonstrated the lifetime distribution of DC-Lyso in lysosomes, suggesting a range of lysosomal polarity under normal physiological conditions (Fig. S34).

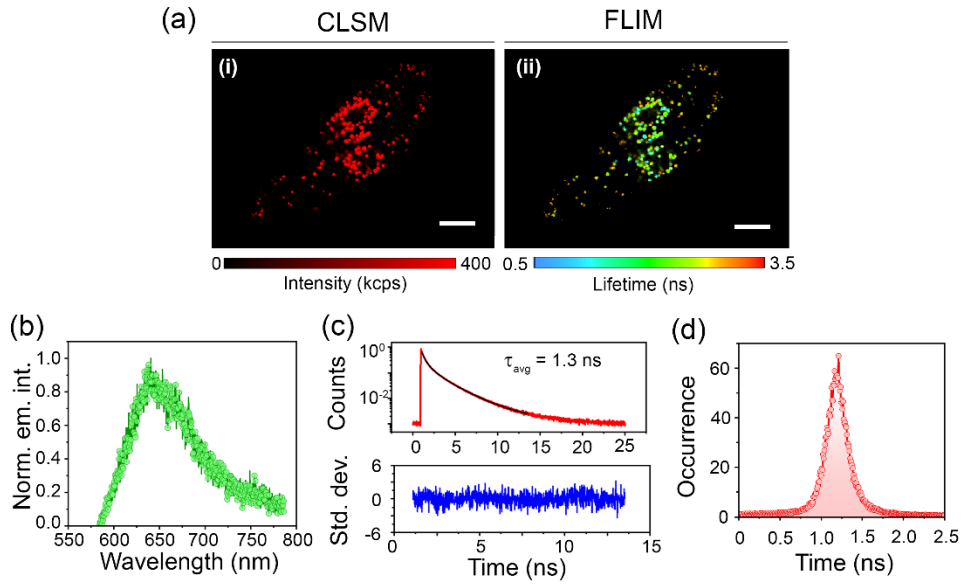

Fig. S34: (a) (i) CLSM and (ii) FLIM images of HeLa cells stained with DC-Lyso (λ_{ex} = 405 nm, λ_{em} = 425 - 800 nm); scale = 10 μm. Intracellular (b) emission profile, (c) lifetime decay trace and corresponding residuals, and (d) the lifetime histogram of DC-Lyso.

Long-term imaging using DC-Lyso:

DC-Lyso exhibited excellent lysosome retention ability and could be used for lysosome imaging for 4 days upon single-time incubation (Fig. S35).

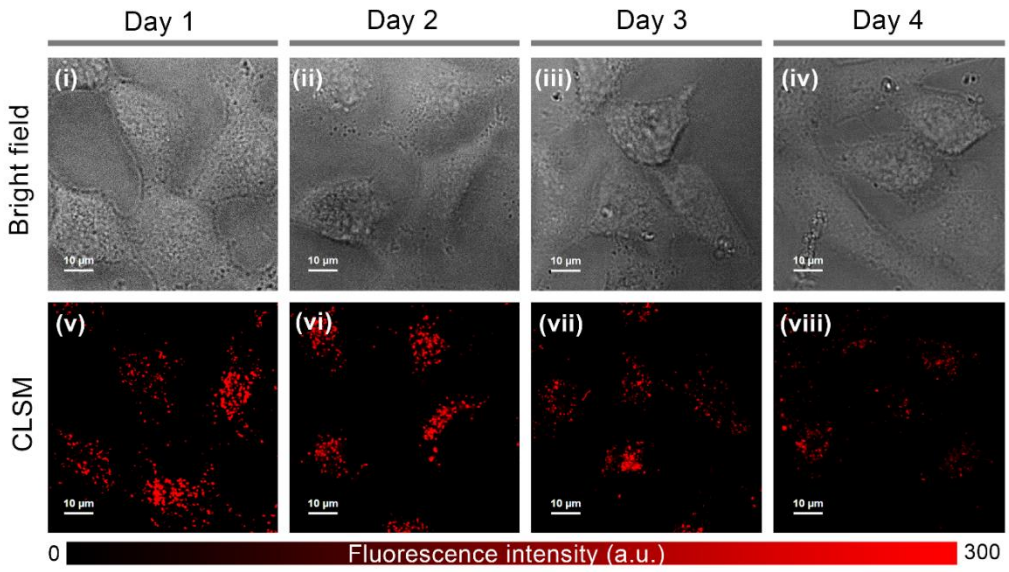

Fig. S35: Long-term imaging of HeLa cells up to 4 days employing DC-Lyso for single-time incubation (10 min). Confocal laser scanning microscopy (CLSM) images of HeLa cells: (i - iv) bright field images, (v - viii) corresponding fluorescence images (λ_{ex} = 405 nm, λ_{em} = 488 - 800 nm) for different days; scale = 10 μm; intracellular fluorescence intensity scale of DC-Lyso is shown.

VII. Probing lysosomal polarity: Dynamics and autophagy

Pseudocolour confocal imaging of DC-Lyso stained HeLa cells over a period of 24 min demonstrated the intracellular lysosomal motions (Fig. S36). The merged images at different imaging time points revealed the different spatial distributions of lysosomes (Fig. S36).

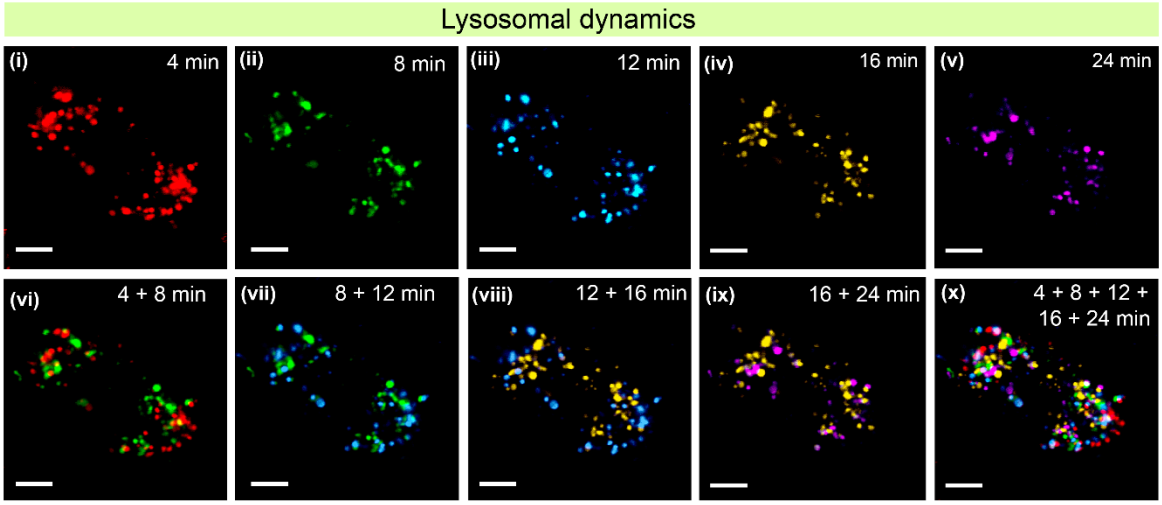

Fig. S36: Pseudo-color-CLSM images revealing lysosomal dynamics in live HeLa cells stained with DC-Lyso (λ_{ex} = 405 nm, λ_{em} = 425 - 800 nm) at different time intervals: (i) 4, (ii) 8, (iii) 12, (iv) 16, and (v) 24 min. The merged images of (vi) i and ii, (vii) ii and iii, (viii) iii and iv, (ix) iv and v, and (x) i to v depict the dynamic nature of lysosomes in live cells; scale = 8 μm.

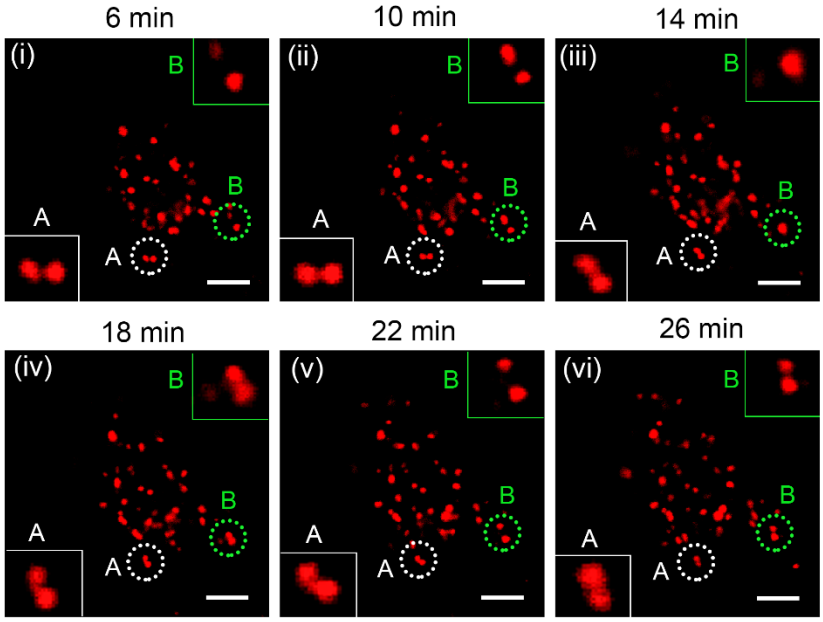

Fig. S37: Tracking the lysosomal dynamics in DC-Lyso stained HeLa cells (λ_{ex} = 405 nm, λ_{em} = 425 - 800 nm); images taken at (i) 6 min, (ii) 10 min, (iii) 14 min, (iv) 18 min, (v) 22 min, and (vi) 26 min after staining. The transient lysosomal movements and associated (A) fusion (white dotted circle, enlarged in white box) and (B) kiss and run (green dotted circle, enlarged in the green box) are depicted; scale = 4 μm.

Closely examining a selected portion of DC-Lyso stained HeLa cells through time-lapse imaging also demonstrated its ability to track the transient lysosomal movements and associated fusion and kiss and run processes (Fig. S37).

Autophagy assay:

The emergence of significant blue fluorescence signals originated from the proprietary fluorescent autophagosome marker (MAK138, Sigma-Aldrich) only in either LPS or CCCP-treated cells confirmed the occurrence of selective autophagy, *i.e.*, lipophagy and mitophagy, respectively, in HeLa cells (Fig. S38).[7,8]

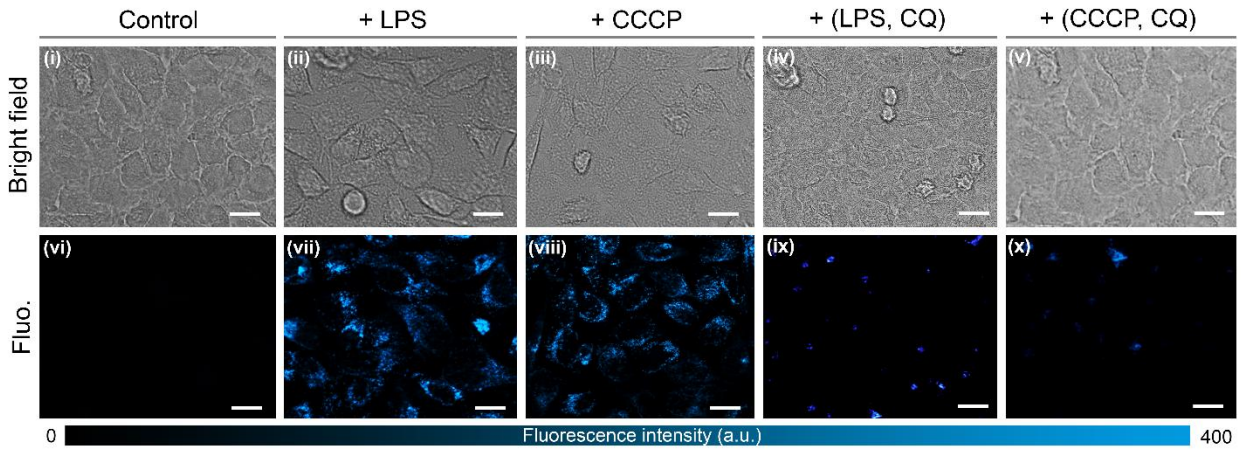

Fig. S38: Fluorescence microscopy images for the determination of autophagy in HeLa cells; (i - v) bright field images and (vi - x) fluorescence images (λ_{ex} = 335 - 383 nm, λ_{em} = 480 - 540 nm). HeLa cells incubated with (i, vi) only Dulbecco's Modified Eagle Medium (DMEM, control), (ii, vii) lipopolysaccharide (LPS, 1 mg mL^{-1}), and (iii, viii) carbonyl cyanide *m*-chlorophenyl hydrazone (CCCP, 10 µM) depict fluorescence signals arising from LPS and CCCP-treated cells and confirm autophagy. The reduction of fluorescence intensity in cells coincubated with (iv, ix) LPS and chloroquine (CQ, 10 µM) and (v, x) CCCP and CQ (10 µM) confirms restricted induction of lipophagy (LPS-treatment) and mitophagy (CCCP-treatment), respectively, in the presence of autophagy inhibitor CQ; scale = 10 µm. A common intensity scale for the fluorescence images is also shown.

Lysosome-lipid droplets interaction:

Interorganelle interactions have been probed during the lipophagy process, where the damaged lipid droplets are engulfed by lysosomes for further degradation.[20] To visualize the lysosomal polarity changes during lipophagy, HeLa cells were treated with DC-Lyso and BODIPY 493/503 (Fig. S39, Fig. S40). Under lipophagic conditions, the Pearson's correlation coefficient of DC-Lyso and BODIPY 493/503 was enhanced significantly than the control set of cells (~2 times, Fig. S41). Moreover, distinct lifetime changes suggested the decreased polarity of lysosomes during the initial stages of lipophagy and the subsequent enhancement (Fig. S40).[20] However, the control cells did not show any significant lifetime or polarity changes in the DC-Lyso channel (Fig. S39, S40b, 40c).

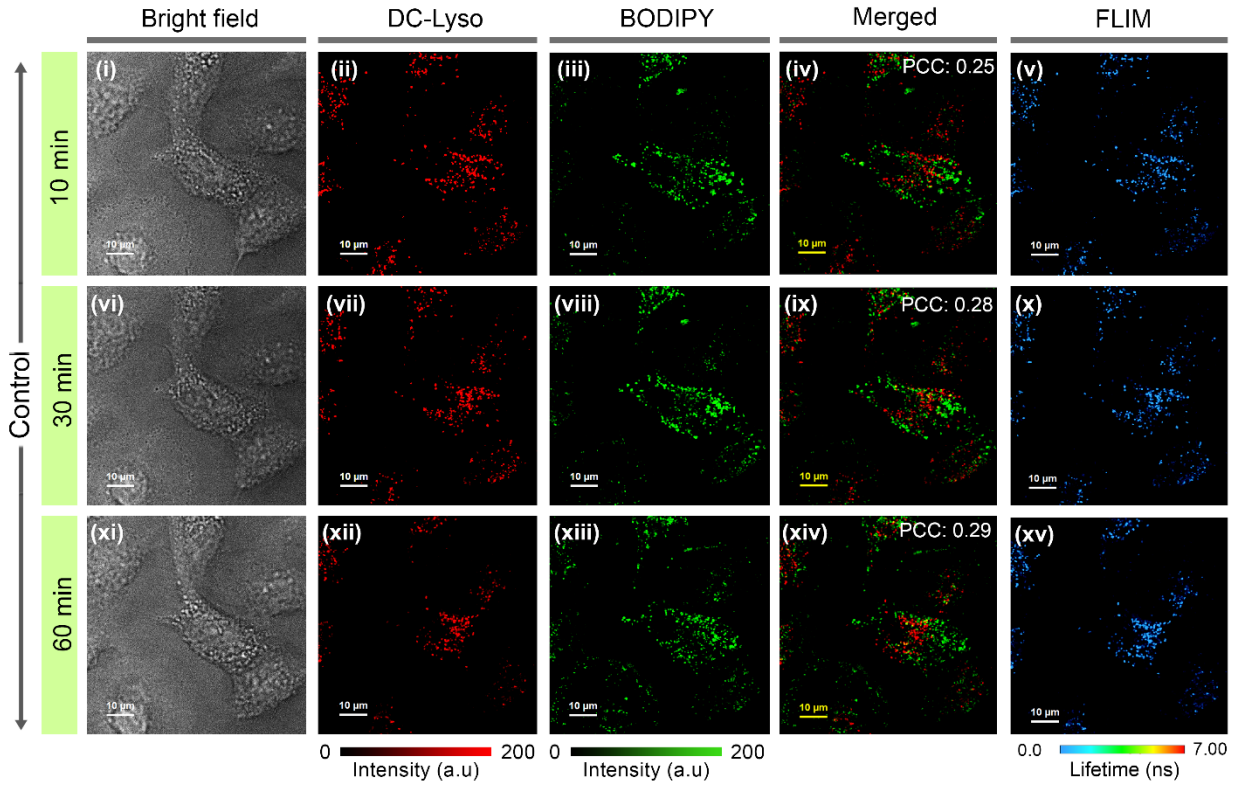

Fig. S39: Time-lapse confocal laser scanning microscopy (CLSM) imaging of lysosome-lipid droplet interactions in a control set of HeLa cells; (i, vi, xi) bright field images, cells incubated with (ii, vii, xii) DC-Lyso (λ_{ex} = 405 nm, λ_{em} = 620 - 660 nm), (iii, viii, xiii) commercial lipid droplet tracker dye, BODIPY 493/503 (BDPY, λ_{ex} = 470 nm, λ_{em} = 520 - 540 nm), and (iv, ix, xiv) corresponding merged images depict the insignificant variation of Pearson's correlation coefficient (PCC). (v, x, xv) Corresponding FLIM images of DC-Lyso channel depict no significant change in the average fluorescence lifetime in lysosomes; scale = 10 µm. A common intensity scale and a lifetime scale for CLSM and FLIM images, respectively, are shown.

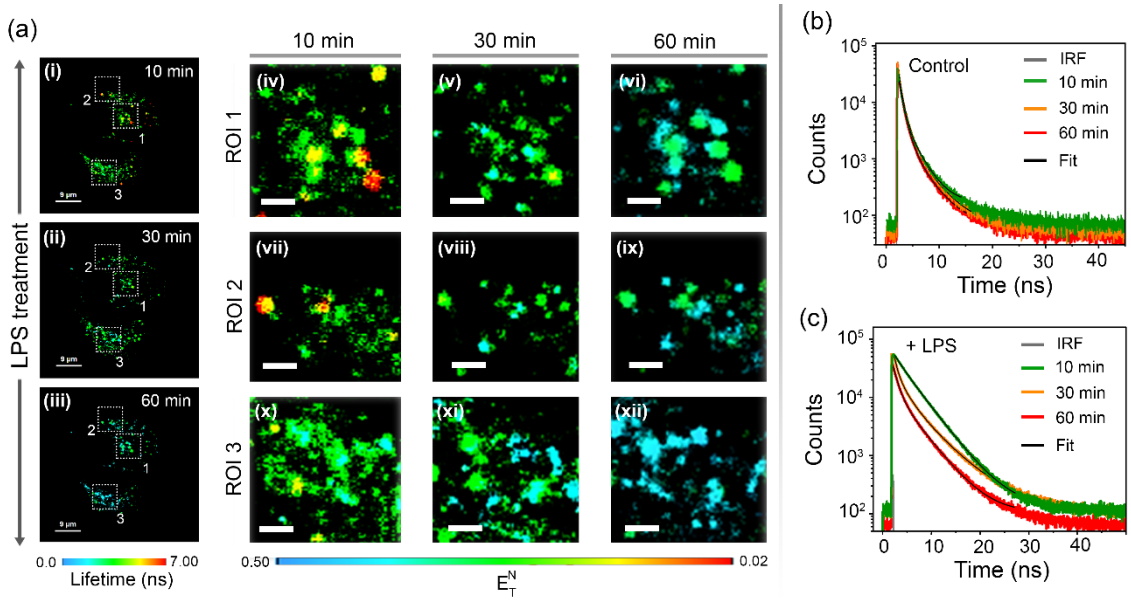

Fig. S40: Time-lapse FLIM imaging of lysosome-lipid droplet interaction (lipophagy) in lipopolysaccharide (LPS)-treated HeLa cells incubated with (i - iii) DC-Lyso (λ_{ex} = 405 nm, λ_{em} = 620 - 660 nm), depicting the fluorescence lifetime variation; scale = 9 μm. (iv - xii) The zoomed images of region of interest (ROI) depicted in (i - iii) further illustrate the lifetime and polarity variation of DC-Lyso in lysosomes under lipophagy; scale = 2 μm. The polarity variations are depicted using the Reichardt's normalized polarity parameter (E_T^N). Intracellular decay traces of DC-Lyso (λ_{ex} = 405 nm, λ_{em} = 620 - 660 nm) stained HeLa cells under (b) control and (c) lipophagy, *i.e.*, LPS-treated conditions at different time points, depicting the variation of decay times only under lipophagy.

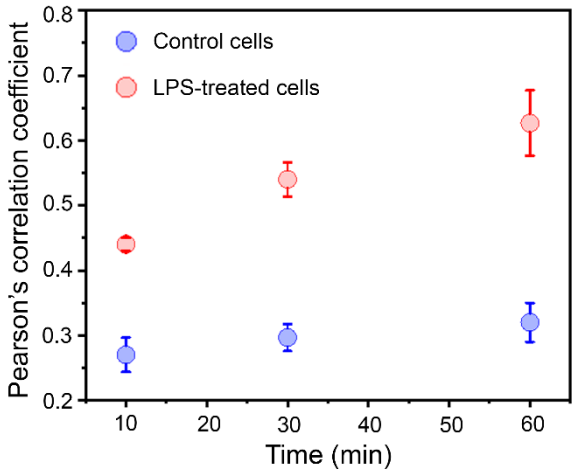

Fig. S41: Time-dependent variation of Pearson's correlation coefficient (PCC) of DC-Lyso and BODIPY 493/503 in control set of HeLa cells (without lipopolysaccharide treatment, blue) and lipopolysaccharide-treated HeLa cells (red) at 10, 30, and 60 min after incubation; error bars are presented based on three independent sample set measurements (n = 3) taking the whole frame analysis in consideration.

Lysosome-mitochondria interaction:

To visualize the lysosomal polarity changes during mitophagy, HeLa cells were treated with DC-Lyso and MTG (Fig. S42, Fig. S43). The control cells did not show any significant lifetime or polarity changes in the DC-Lyso channel (Fig. S42). However, under mitophagy conditions (CCCP treatment), distinct lifetime changes in the DC-Lyso channel suggested the enhanced polarity of lysosomes during mitophagy (Fig. S43-S46).[20]

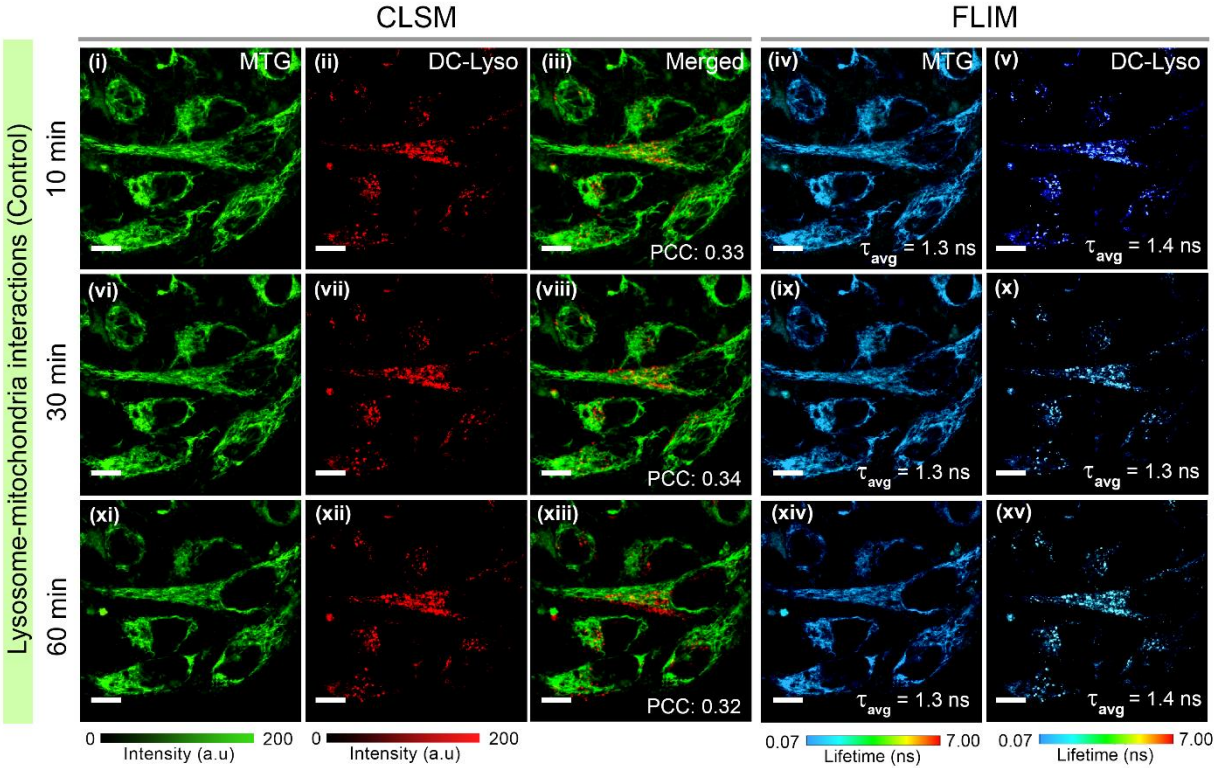

Fig. S42: Time-lapse imaging of lysosome-mitochondria interaction in HeLa cells incubated with (i, vi, xi) commercial mitochondria tracker dye, MitoTracker™ Green (MTG, λ_{ex} = 470 nm, λ_{em} = 500 - 540 nm), (ii, vii, xii) DC-Lyso (λ_{ex} = 405 nm, λ_{em} = 620 - 660 nm), and (iii, viii, xiii) corresponding merged images show no significant change in the Pearson's correlation coefficient. Corresponding fluorescence lifetime imaging microscopy (FLIM) images of HeLa cells for the (iv, ix, xiv) MTG and (v, x, xv) DC-Lyso channels reveal the insignificant variation of fluorescence lifetime for DC-Lyso in lysosomes under normal physiological conditions; scale = 10 μm. A common intensity scale and a lifetime scale for CLSM and FLIM images, respectively, are shown.

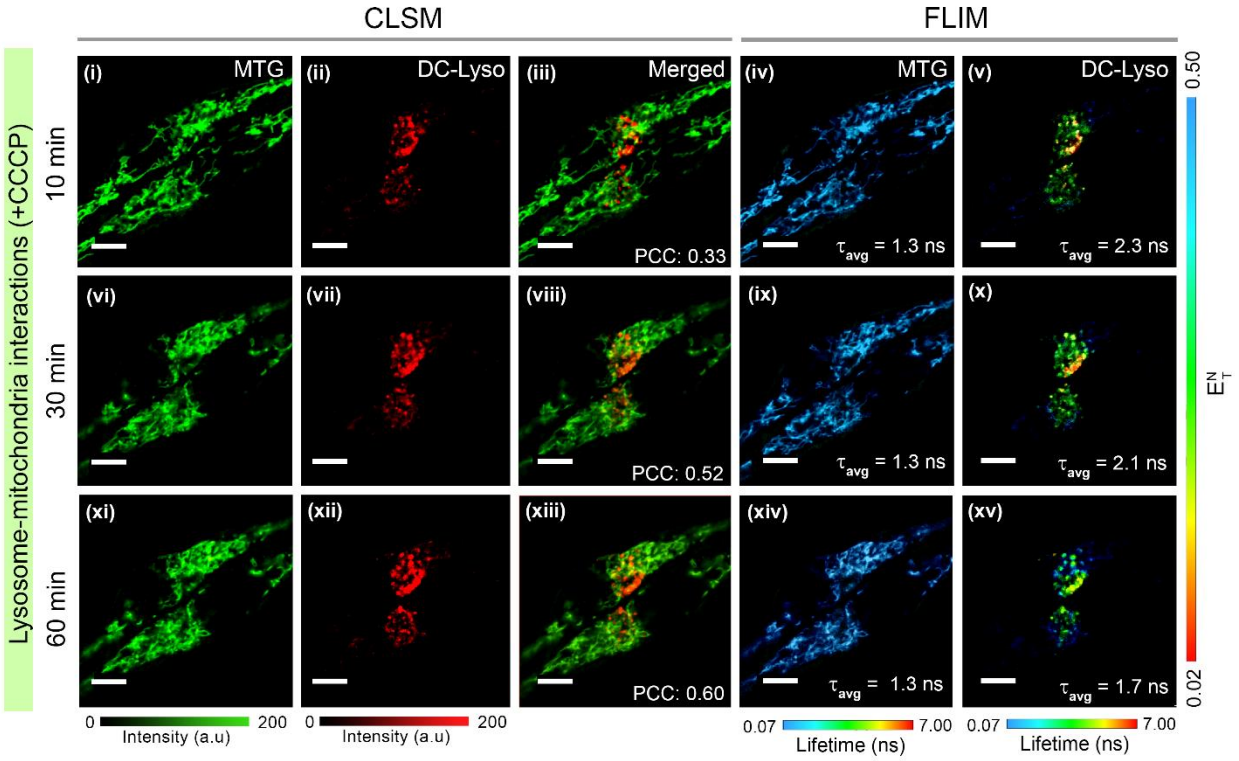

Fig. S43: Time-lapse imaging of lysosome-mitochondria interaction during mitophagy in carbonyl cyanide *m*-chlorophenyl hydrazone (CCCP)-treated HeLa cells incubated with (i, vi, xi) commercial mitochondria tracker dye, MTG (λ_{ex} = 470 nm, λ_{em} = 500 - 540 nm), (ii, vii, xii) DC-Lyso (λ_{ex} = 405 nm, λ_{em} = 620 - 660 nm), and (iii, viii, xiii) corresponding merged images show a gradual increase in the Pearson's correlation coefficient (PCC), indicating lysosome-mitochondria interaction with time. Corresponding fluorescence lifetime imaging microscopy (FLIM) images of HeLa cells for (iv, ix, xiv) MTG and (v, x, xv) DC-Lyso channels again suggest a significant variation of fluorescence lifetime for DC-Lyso in lysosomes under CCCP treatment (mitophagy); scale = 7 μm. The polarity variation is depicted using the Reichardt's normalized polarity parameter (E_T^N), revealing the increase of lysosomal polarity over time during mitophagy. A common intensity scale and a lifetime scale for CLSM and FLIM images, respectively, are shown.

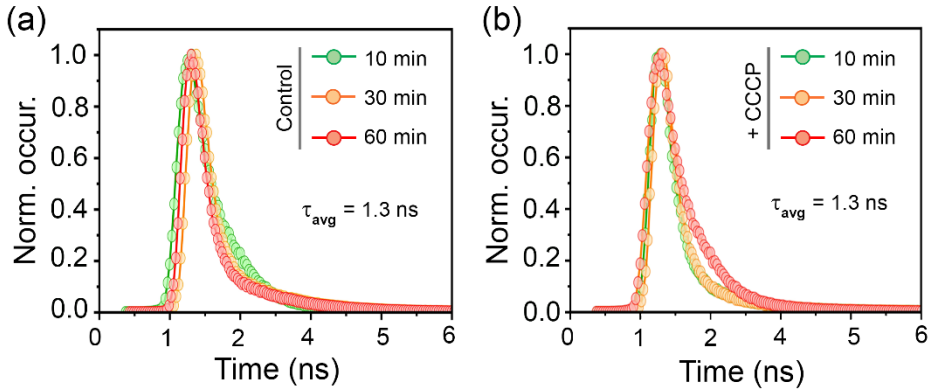

Fig. S44: Lifetime histograms of HeLa cells treated with MTG under (a) control and (b) CCCP-treated conditions at different time points.

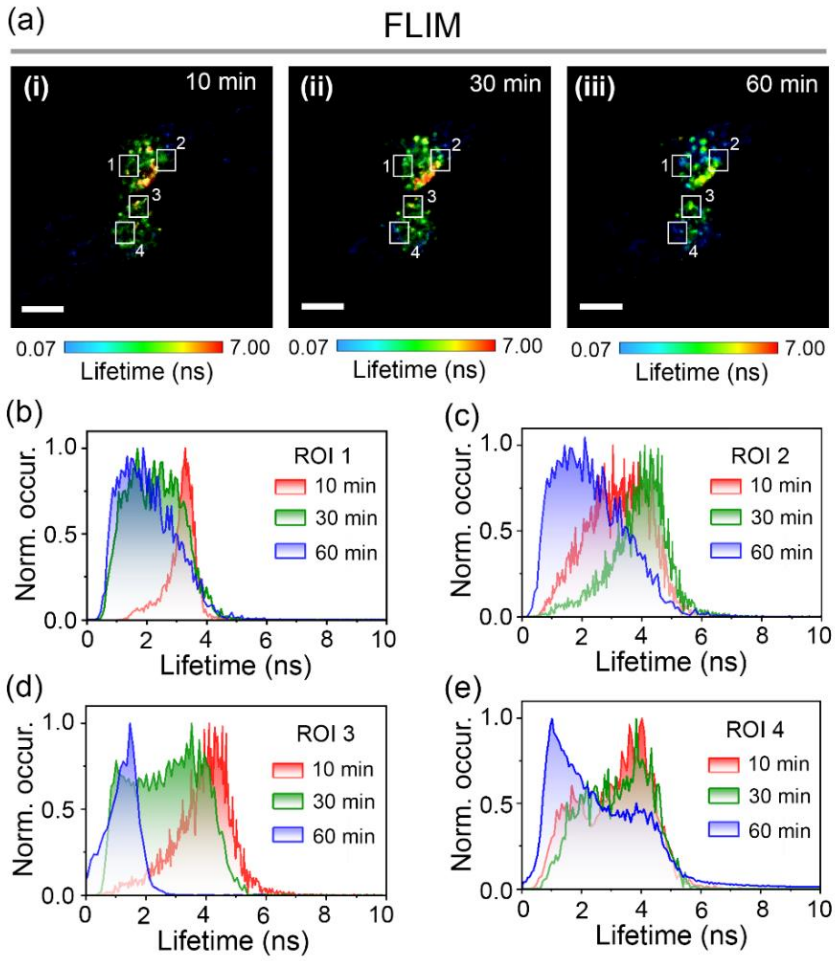

Fig. S45: (a) Time-lapse fluorescence lifetime imaging microscopy (FLIM) images of carbonyl cyanide *m*-chlorophenyl hydrazone (CCCP)-treated HeLa cells stained with DC-Lyso (λ_{ex} = 405 nm, λ_{em} = 620 - 660 nm); images taken at (i) 10, (ii) 30, and (iii) 60 min after incubation with CCCP; scale = 7 μm. (b - e) Representative lifetime histograms of DC-Lyso of the region of interests (ROIs) depicted in (a) for 10, 30, and 60 min after CCCP treatment.

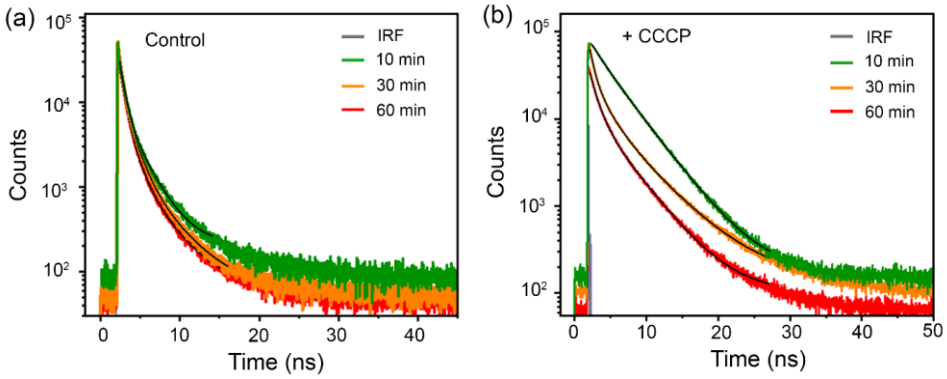

Fig. S46: Intracellular decay traces of DC-Lyso (λ_{ex} = 405 nm, λ_{em} = 620 - 660 nm) stained HeLa cells under (a) control and (b) mitophagy, *i.e.*, CCCP-treated conditions at different time points.

VIII. Lysosomal polarity as an indicator of aging in *Caenorhabditis elegans*

Imaging of *Caenorhabditis elegans*:

Specific staining of *Caenorhabditis elegans* (*C. elegans*) by DC-Lyso was observed by fluorescence microscopy (Fig. S47, Fig. S48). In comparison, the unstained *C. elegans* showed no fluorescence signals (Fig. S47, iv).

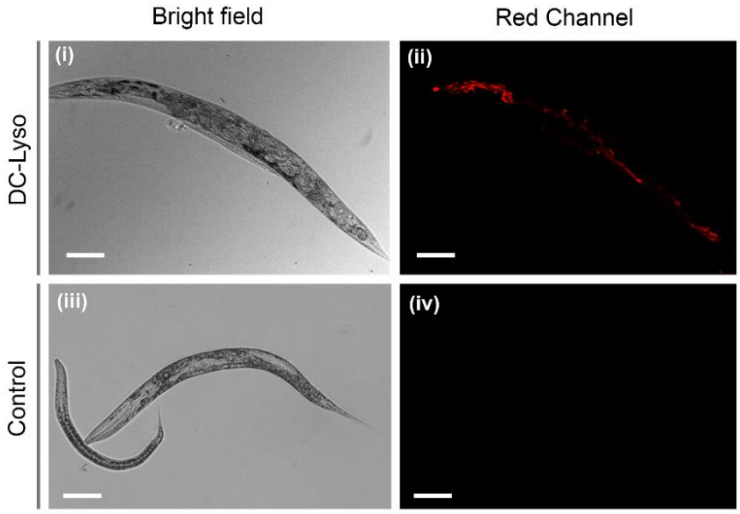

Fig. S47: Imaging of *Caenorhabditis elegans* (*C. elegans*): (i, ii) stained with DC-Lyso (2 μM, λ_{ex} = 405 nm, λ_{em} = 620 - 660 nm), (iii, iv) without DC-Lyso staining. (i, iii) Bright field and (iii, iv) fluorescence images; scale = 100 μm.

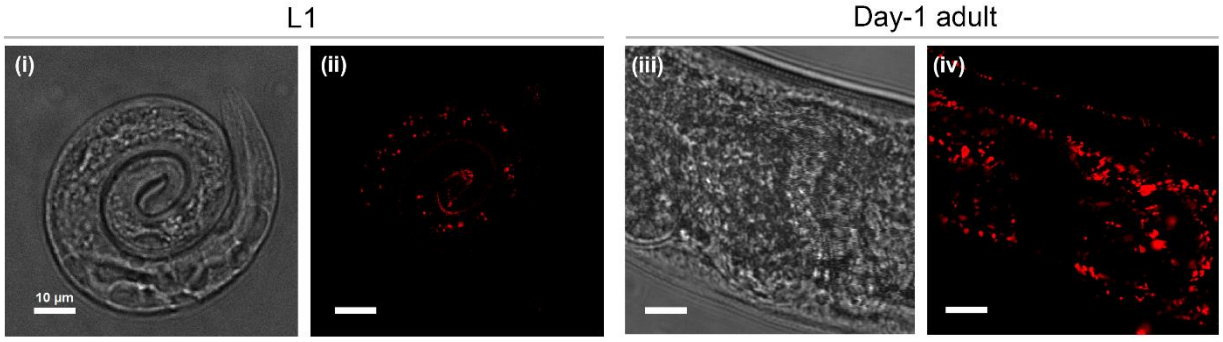

Fig. S48: CLSM imaging of wild-type (N2) *C. elegans* (i, ii) L1, and (iii, iv) day-1 adult stages (intestinal region) incubated with DC-Lyso; (i, iii) bright field and (ii, iv) fluorescence images (λ_{ex} = 405 nm, λ_{em} = 425 - 800 nm); scale = 10 μm.

Lysosome-related organelle targeting by DC-Lyso:

The lysosome-related organelle specificity of DC-Lyso in *C. elegans* was checked using colocalization studies (Fig. S49). Staining with commercial tracker dyes revealed the lysosome-targeting ability of DC-Lyso in *C. elegans* (Fig. S49).

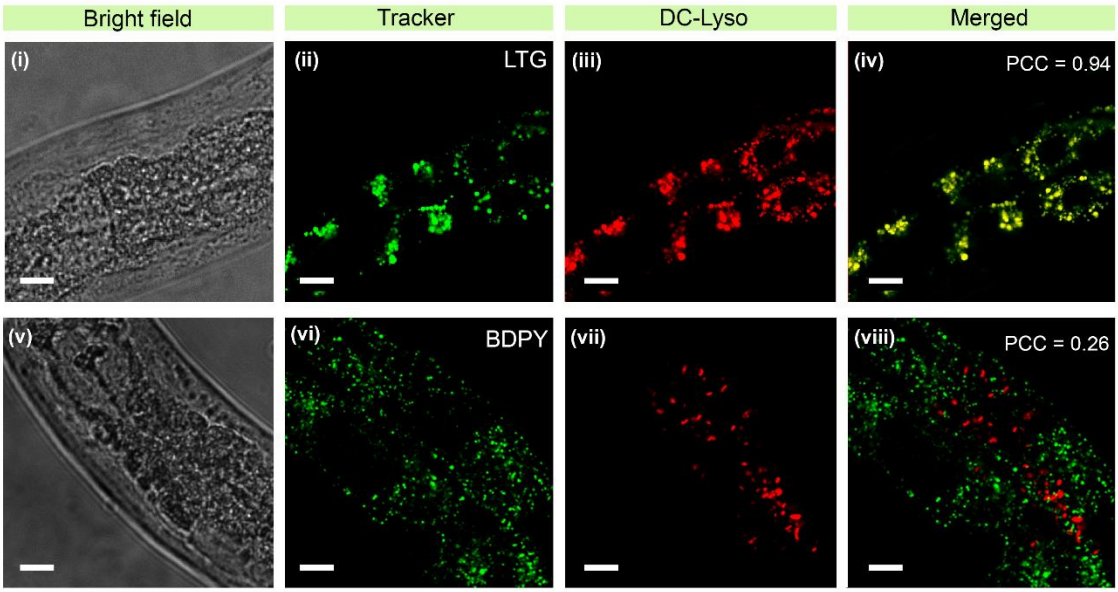

Fig. S49: Colocalization studies using CLSM in the intestinal region of wild-type (N2) *C. elegans* coincubated with DC-Lyso and commercially available organelle tracker dyes; (i, v) bright field images, *C. elegans* stained with (ii) LTG (λ_{ex} = 470 nm, λ_{em} = 500 - 540 nm), (vi) BODIPY 493/503 (BDPY, λ_{ex} = 470 nm, λ_{em} = 500 - 540 nm), (iii, vii) DC-Lyso (λ_{ex} = 405 nm, λ_{em} = 620 - 660 nm), and the merged images of (iv) ii and iii, (viii) vi and vii, depict a high PCC value of 0.94 only for DC-Lyso with LTG, suggesting lysosome-related organelle targeting ability of the probe in the multicellular model organism; scale = 10 μm.

Probing aging in *C. elegans*:

The potential of DC-Lyso to monitor cellular polarity was further explored in different developmental stages (L2 to day-1 adult) of wild-type (N2 strain) and short-lived (*daf-16*) *C. elegans* (Fig. S50, Fig. S51). The FLIM images showed the gradual decrease of the fluorescence lifetime of DC-Lyso, revealing the enhanced polarity of lysosome-related organelles in *C. elegans* with aging (Fig. S50, Fig. S51).

The aging-related polarity tracking ability of DC-Lyso was further compared by staining wild-type *C. elegans* with DC-Lyso and LTR during their developmental stages. The lysosomal lifetime changes were only observable for DC-Lyso due to its polarity-sensitive tunable emission property (Fig. S52).

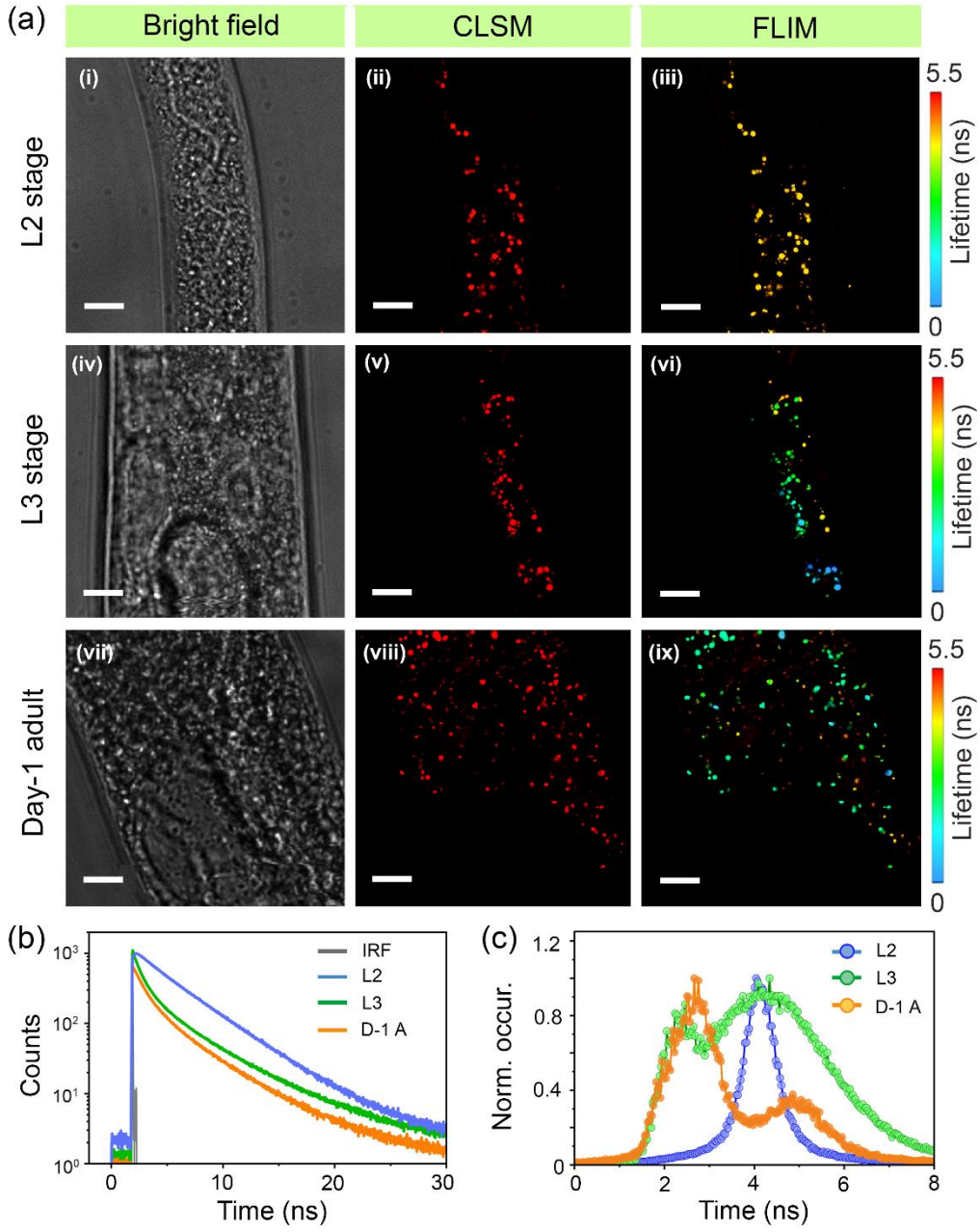

Fig. S50: Probing the lysosomal polarity changes in the intestinal region of wild-type (N2) *C. elegans* stained with DC-Lyso (λ_{ex} = 405 nm, λ_{em} = 425 - 800 nm). (a) Images of *C. elegans* (i, iv, vii) bright field images, (ii, v, viii) CLSM images, and (iii, vi, ix) FLIM images of (i - iii) L2, (iv - vi) L3, and (vii - ix) day-1 adult (D-1 A) stages of the worm depicting gradual lowering of the fluorescence lifetime; scale = 10 µm. The intracellular (b) decay traces and (c) lifetime histograms of DC-Lyso stained *C. elegans* at different developmental stages (L2, L3, and D-1 A).

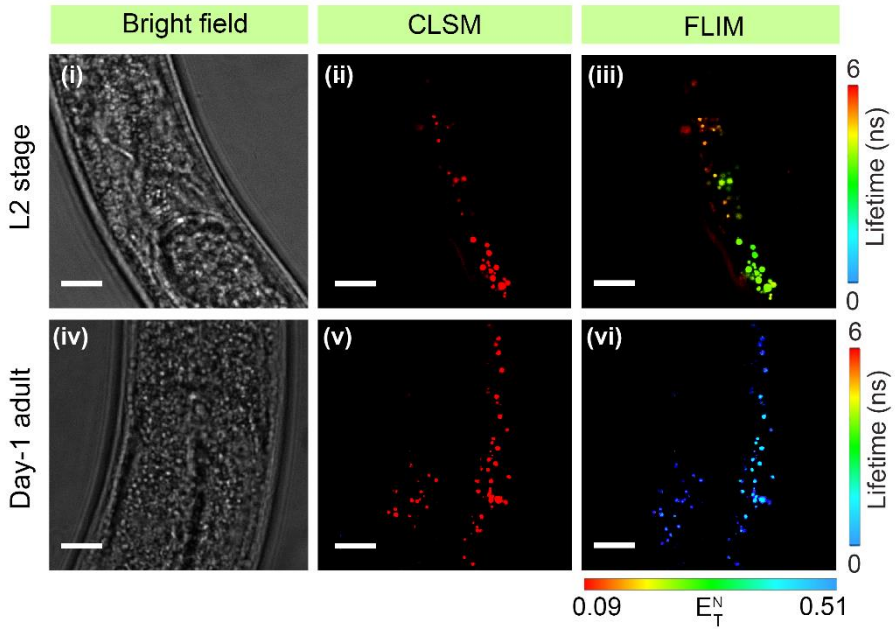

Fig. S51: Probing the lysosomal polarity changes in the intestinal region of mutant (*daf-16*) *C. elegans* stained with DC-Lyso (λ_{ex} = 405 nm, λ_{em} = 425 - 800 nm). Images of *C. elegans* (i, iv) bright field images, (ii, v) CLSM images, and (iii, vi) FLIM images of (i - iii) L2 and (iv - vi) day-1 adult stages of the worm depicting gradual lowering of the fluorescence lifetime. The polarity variation is depicted using Reichardt's normalized polarity parameter (E_T^N), revealing the increase of lysosomal polarity with aging in mutant worms.

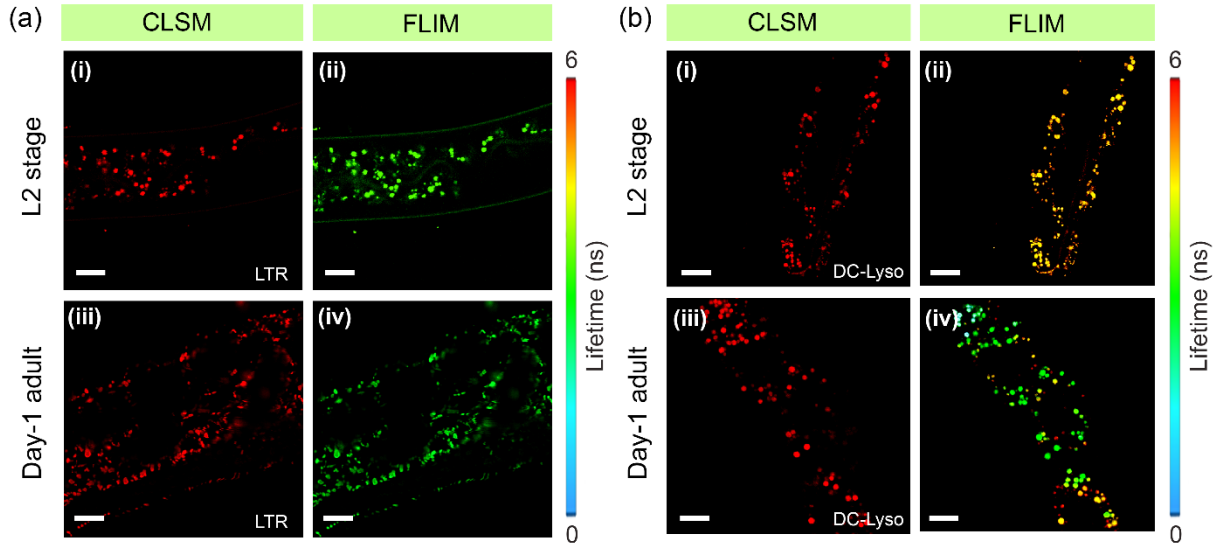

Fig. S52: (a) (i, iii) CLSM and (ii, iv) FLIM images of LTR (λ_{ex} = 530 nm, λ_{em} = 620 - 660 nm) stained (i, ii) L2 and (iii, iv) day-1 adult *C. elegans* (intestinal region). (b) (i, iii) CLSM and (ii, iv) FLIM images of DC-Lyso (λ_{ex} = 470 nm, λ_{em} = 620 - 660 nm) stained (i, ii) L2 and (iii, iv) day-1 adult *C. elegans* (intestinal region); scale = 10 μm. The images depict the polarity sensing ability of DC-Lyso due to its tunable lifetime.

IX. *In vivo* delayed fluorescence imaging

Time-resolved imaging was performed in different cancerous cell lines (HeLa, A549, and CHO) at the microsecond time scale using DC-Lyso nanoparticles, *i.e.*, DCL-NPs in water (Fig. S53). Applying a time-gate of 1 μs, the images depicted bright fluorescence signals, demonstrating the suitability of DCL-NPs for time-gated imaging under biological conditions (Fig. S53).

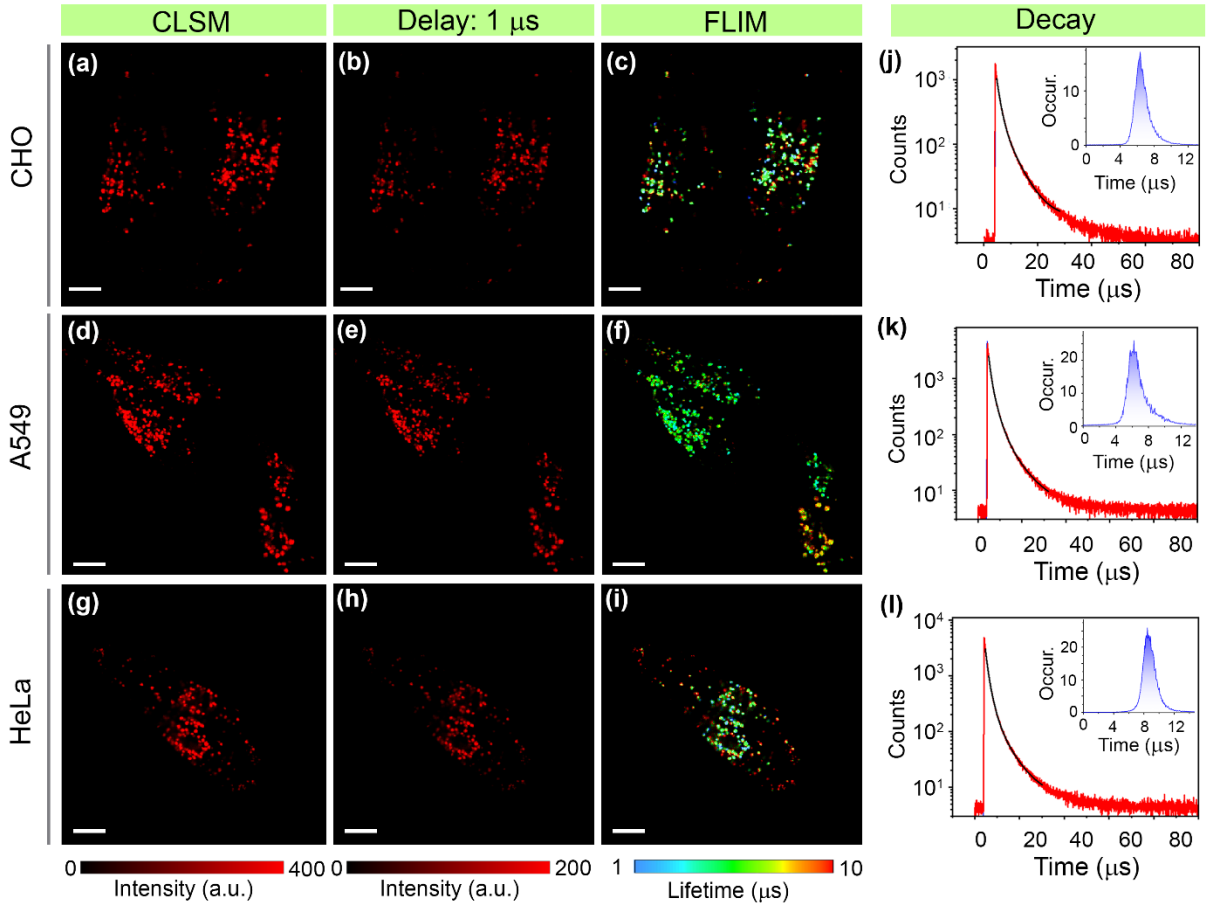

Fig. S53: Time-resolved imaging employing aqueous dispersion of DC-Lyso nanoparticles (DCL-NPs, λ_{ex} = 470 nm, λ_{em} = 488 - 800 nm), (a - c) CHO, (d - f) A549, and (g - i) HeLa cells. (a, d, g) CLSM images with no time delay, (b, e, h) time-gated images after applying a time delay of 1 μs, and (c, f, i) microsecond timescale FLIM images; scale = 10 μm. The corresponding intracellular lifetime decay plots of (j) CHO, (k) A549, and (l) HeLa cells; inset: the fluorescence lifetime histogram of DCL-NPs in the respective cell lines.

X. Comparative table

Table S9: Comparative table comprising lysosome-specific fluorescent and delayed fluorescent molecular probes for elucidating microenvironmental changes during organelle interactions.

No	Probe	λ_{em} (nm)	Incubation time	Organelle interactions	Multiday imaging	Time delay for *in vivo* delayed fluorescence imaging	Probing cellular microenvironment	Ref.
1	DC-Lyso	650	1 min	Lysosome-lipid droplet, lysosome-mitochondria	Up to 4-day imaging by single-time incubation	1 μs	Revealing lysosomal polarity changes as an indicator of lipophagy and mitophagy in cells and aging in *C. elegans* through FLIM	This work
2	Coupa	500/ 650	30 min	Lysosome-mitochondria	NR	NR	Mitochondrial viscosity	21
3	Q-P-Arh	675	1 min	Lysosome-lipid droplet	Up to 3.5-days imaging by single-time incubation	NR	NR	22
4	DCIP	653	10 min	Lysosome-mitochondria	NR	NR	NR	23
5	DCM-NH_2	640	30 min	Lysosome-mitochondria	NR	NR	NR	24
6	Lyso-PXZ-NI	625	1.5 h	Lysosome-specific#	NR	200 ns	NR	25
7	Al-Cz-LT	520	2 h	Lysosome-specific#	NR	1 μs	NR	26

NR: Not reported; # no TADF/long-lived emissive probes have been reported so far depicting interorganelle interactions or probing cellular microenvironments.

XI. Characterization: ^{1}H, ^{13}C-NMR, and mass spectra

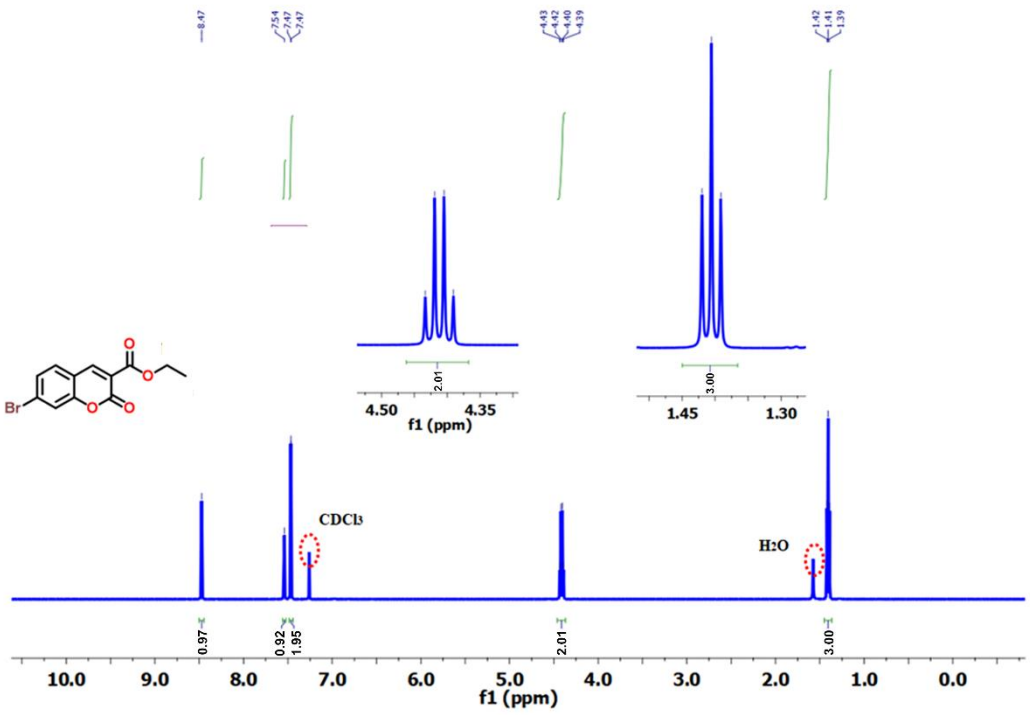

Fig. S54: ^{1}H-NMR spectrum of P1 in $CDCl_3$.

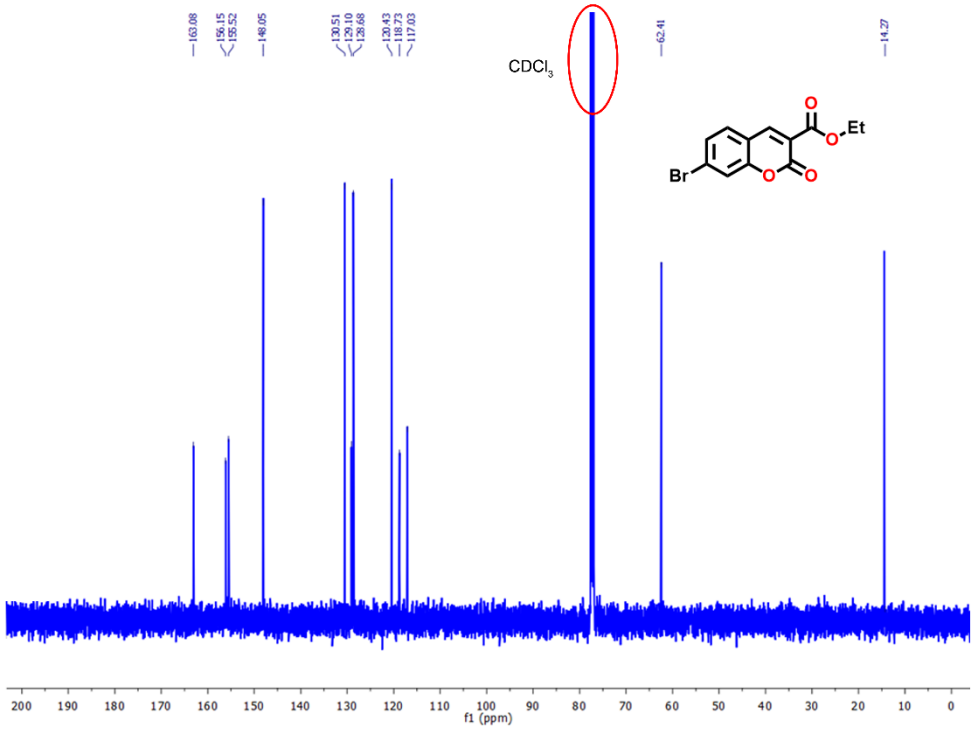

Fig. S55: ^{13}C-NMR spectrum of P1 in $CDCl_3$.

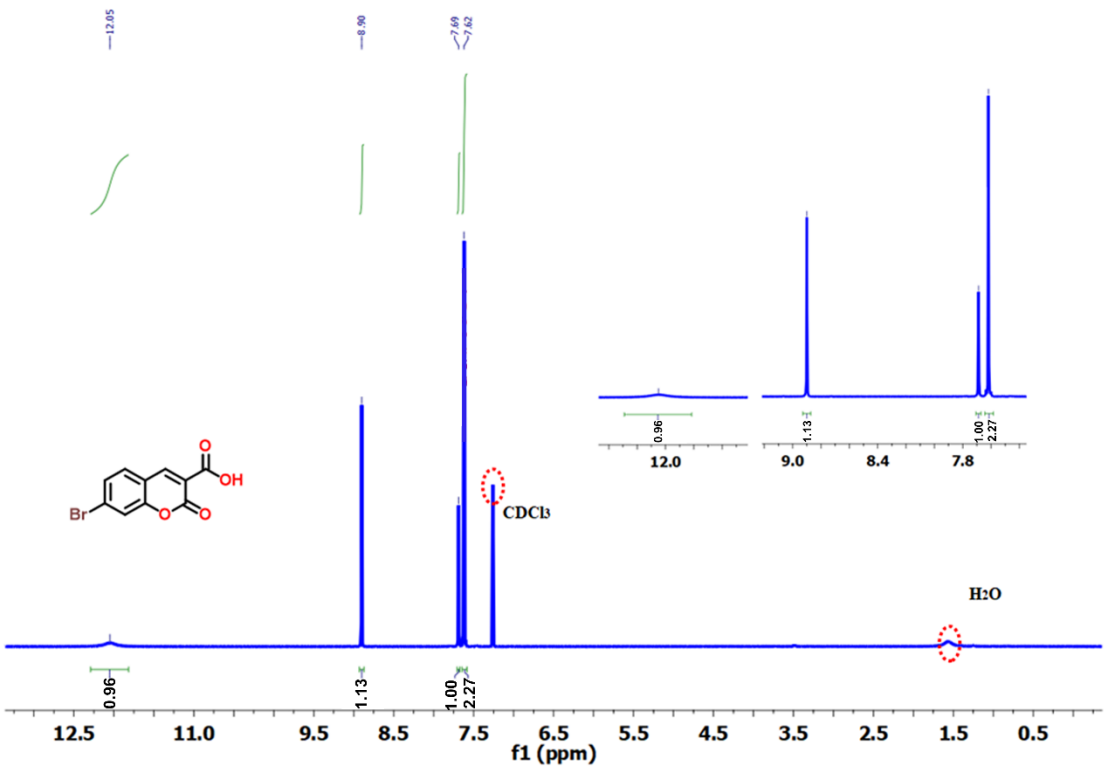

Fig. S56: ^{1}H-NMR spectrum of P2 in $CDCl_3$.

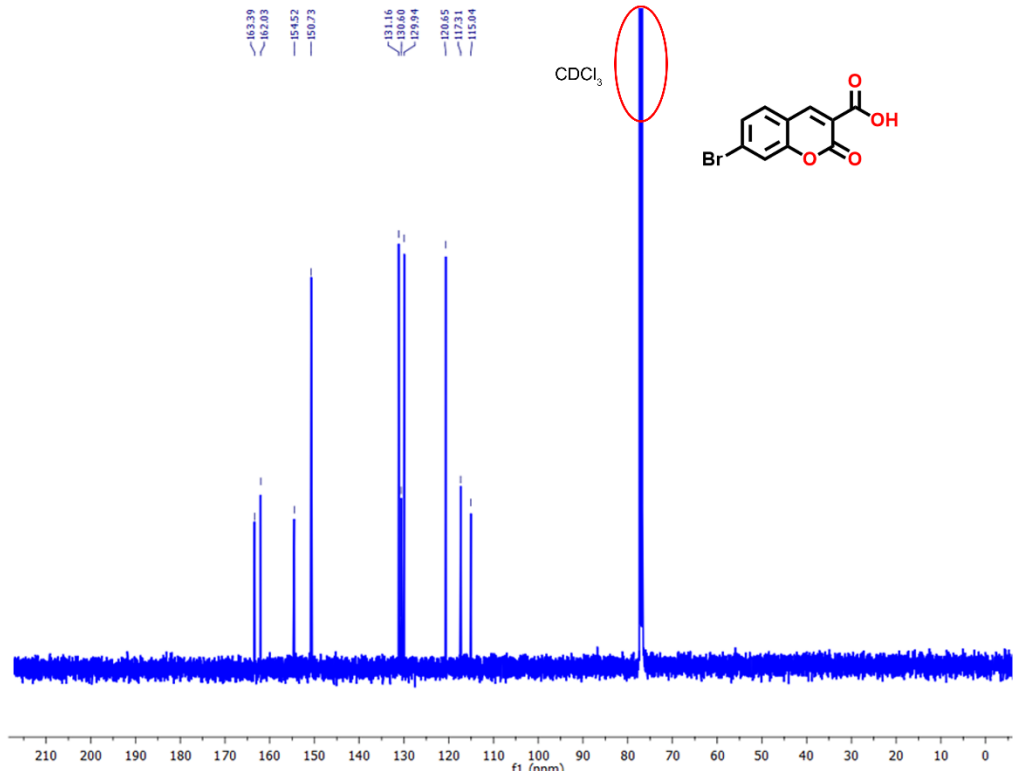

Fig. S57: ^{13}C-NMR spectrum of P2 in $CDCl_3$.

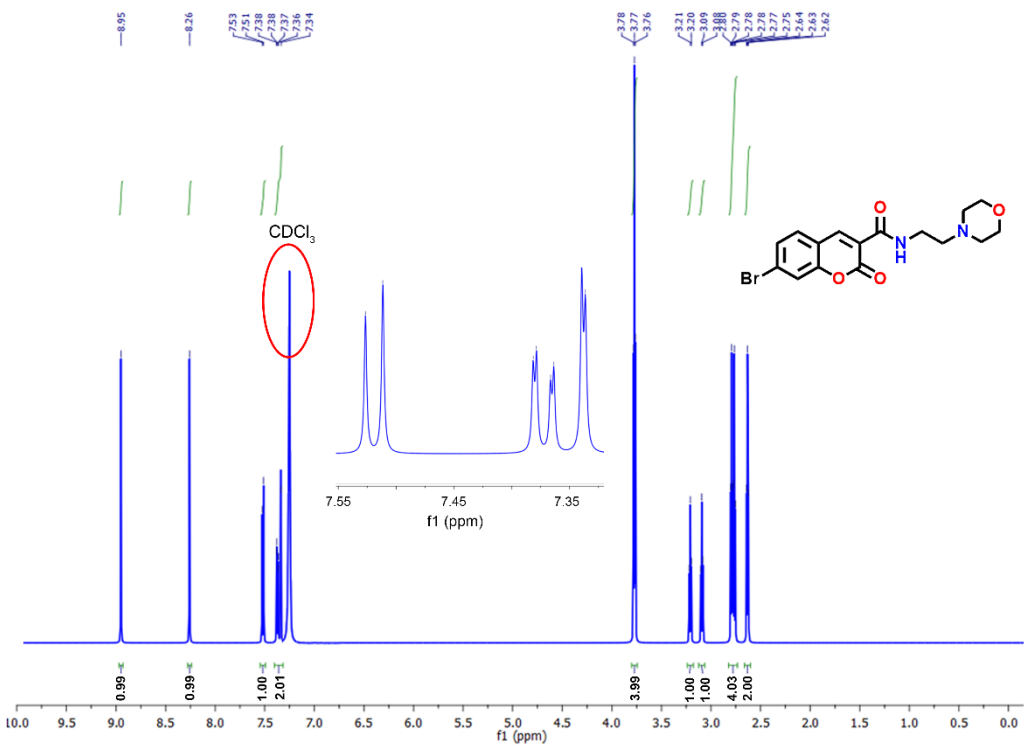

Fig. S58: ^{1}H-NMR spectrum of P3 in $CDCl_3$.

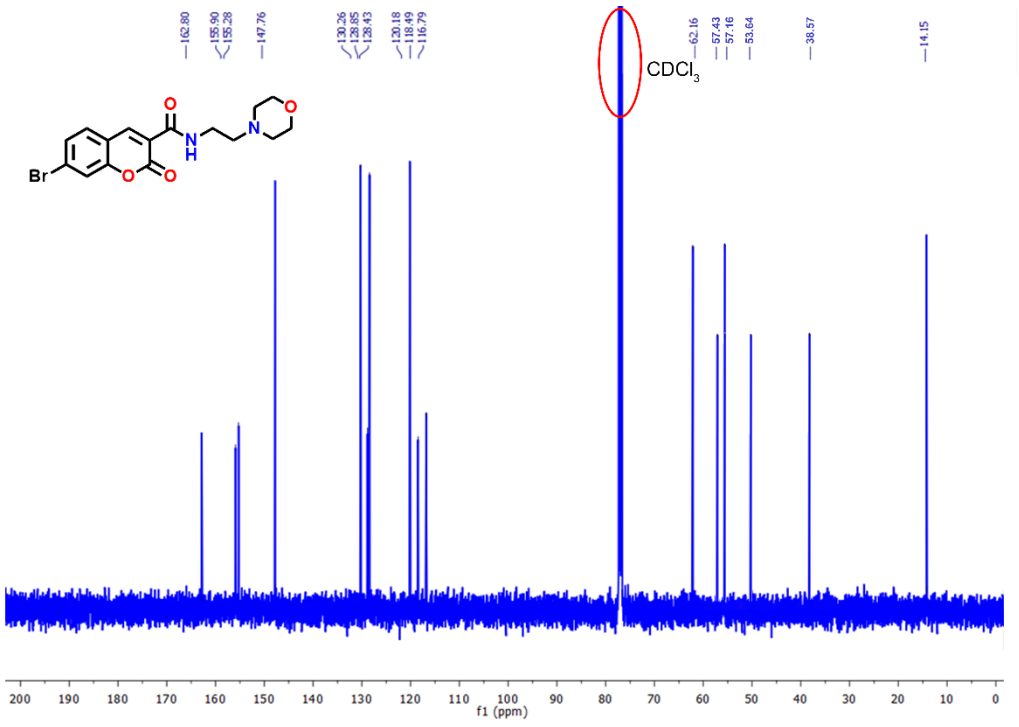

Fig. S59: ^{13}C-NMR spectrum of P3 in $CDCl_3$.

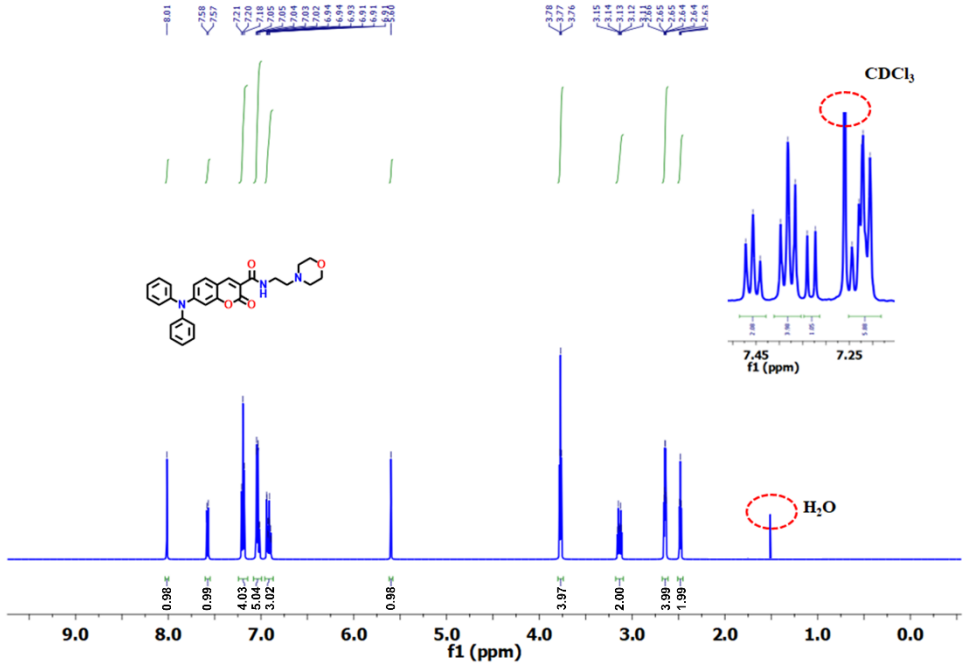

Fig. S60: ^{1}H NMR spectrum of DC-Lyso in $CDCl_3$.

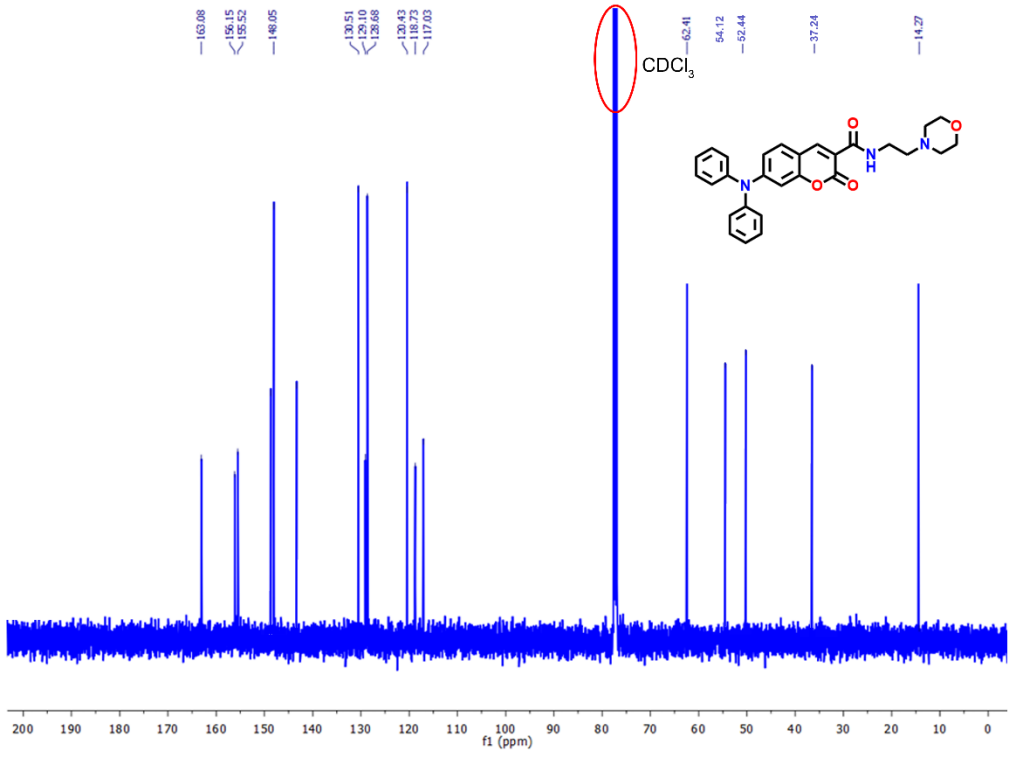

Fig. S61: ^{13}C-NMR spectrum of DC-Lyso in $CDCl_3$.

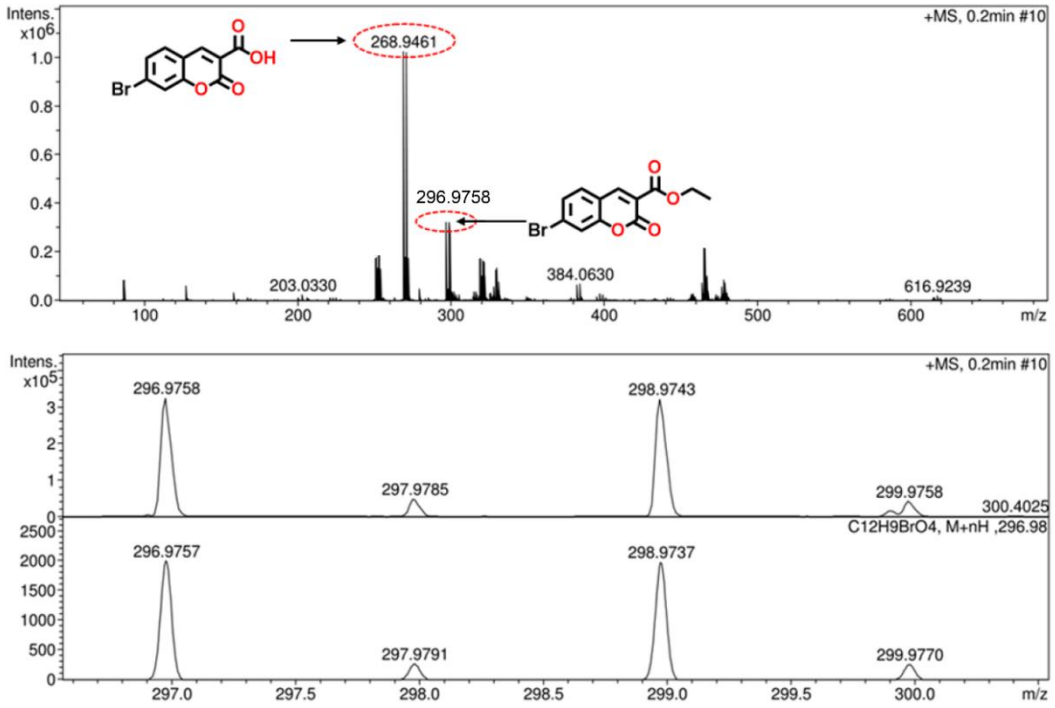

Fig. S62: HRMS data (electrospray ionization, ESI) of P1.

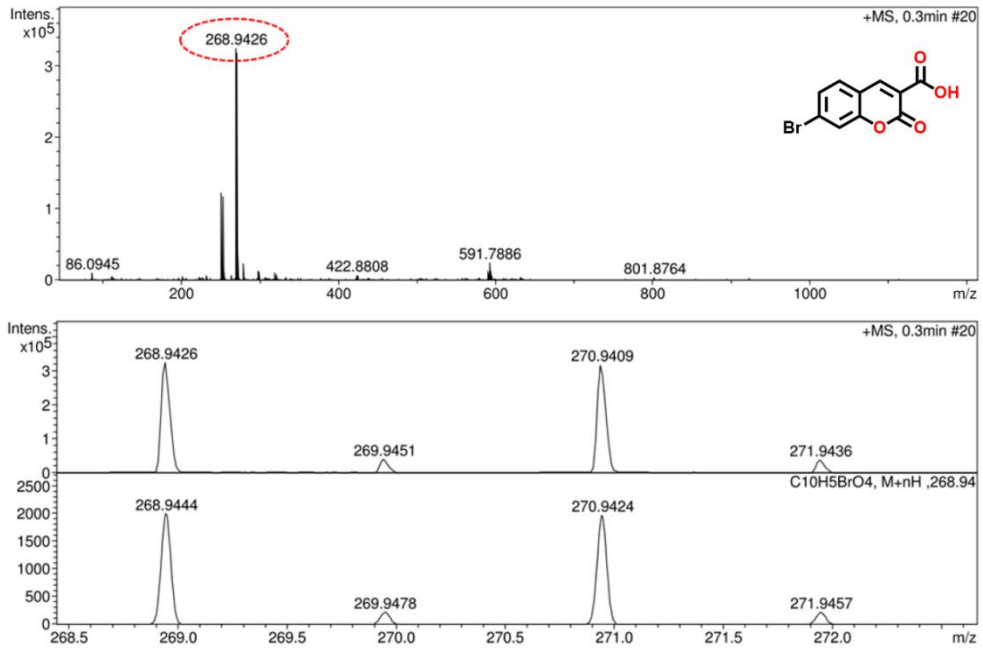

Fig. S63: HRMS data (ESI) of P2.

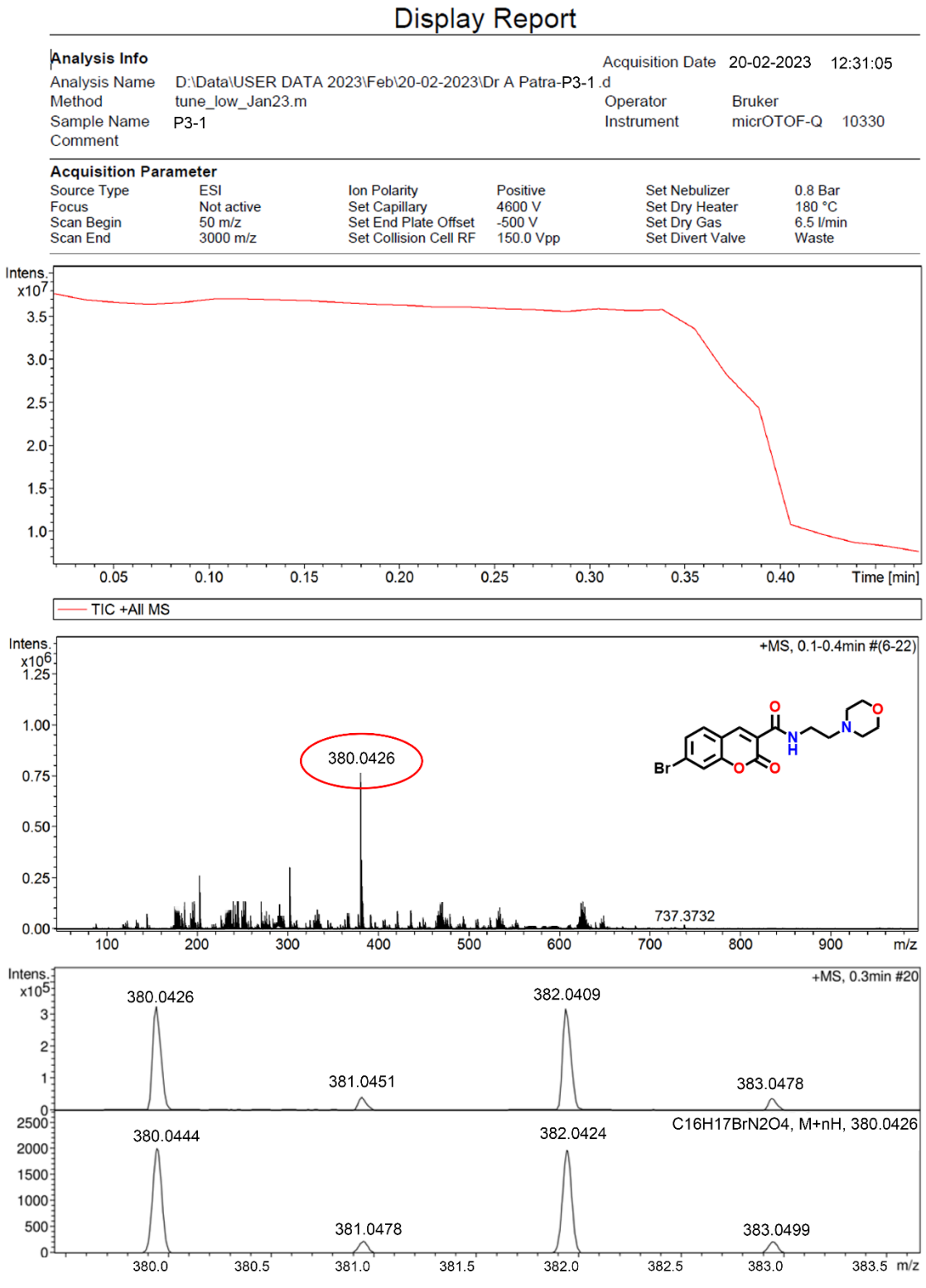

Fig. S64: HRMS data (ESI) of P3.

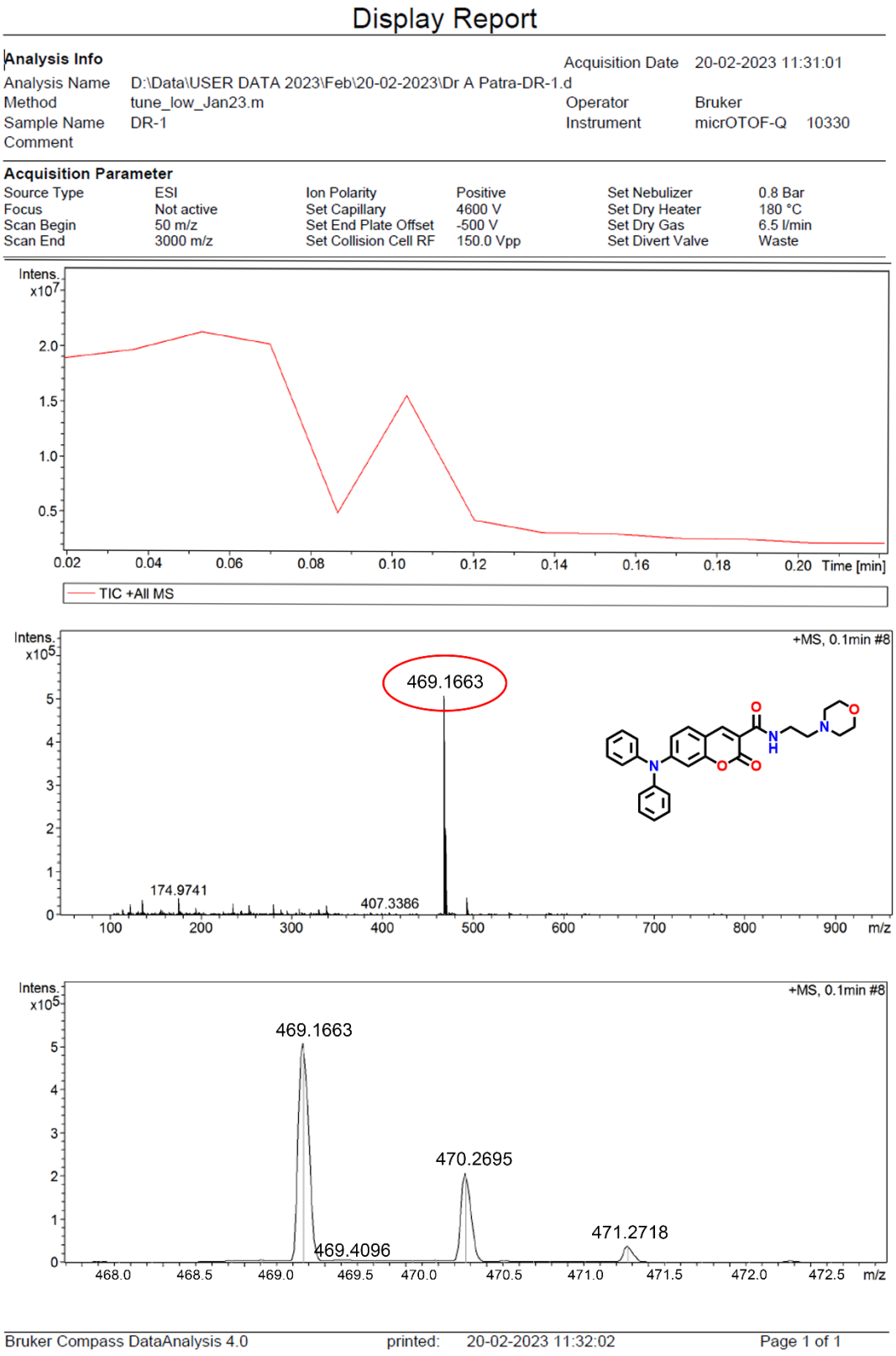

Fig. S65: HRMS data (ESI) of DC-Lyso.

XII. References

1. J. R. Lakowicz, *Principles of Fluorescence Spectroscopy,* Springer, New York, 2006.
2. S. Kundu, A. Chowdhury, S. Nandi, K. Bhattacharyya and A. Patra, *Chem. Sci*. 2021, **12**, 5874.
3. K. Sugano, M. Kansy, P. Artursson, A. Avdeef, S. Bendels, L. Di, G. F. Ecker, B. Faller, H. Fischer, G. Gerebtzoff, H. Lennernaes and F. Senner, *Nat. Rev. Drug Discov.*, 2010, **9**, 597.
4. L. H. Wang, K. G. Rothberg and R. G. Anderson, *J. Cell Biol.*, 1993, **123**, 1107-1117.
5. L. J. Hewlett, A. R. Prescott and C. Watts, *J. Cell Biol.*, 1989, **109**, 2731-2739.
6. C. Donohoe, F. A. Schaberle, F. M. S. Rodrigues, N. P. F. Gonçalves, C. J. Kingsbury, M. M. Pereira, M. O. Senge, L. C. Gomes-da-Silva and L. G. Arnaut, *J. Am. Chem. Soc.* 2022, **144**, 15252-15265.
7. A. Rogalska, A. Gajek, M. Łukawska, I. Oszczapowicz and A. Marczak, *PloS one*, 2018, **13**, e0201296-e0201296.
8. H. Ye, M. Chen, F. Cao, H. Huang, R. Zhan and X. Zheng, *BMC Neurology*, 2016, **16**, 178.
9. S. Brenner, *Genetics*. 1974, **77**, 71.
10. H. J. Park, C. W. Song, S. Sarkar, Y. W. Jun, Y. J. Reo, M. Dai and K. H. Ahn, *Chem. Commun*., 2020, **56**, 7025.
11. Y. Xie, J. T. Husband, M. Torrent-Sucarrat, H. Yang, W. Liu and R. K. O'Reilly, *Chem. Commun.*, 2018, **54**, 3339.
12. Z. R. Grabowski, K. Rotkiewicz and W. Rettig, *Chem. Rev*., 2003, **103**, 3899.
13. C. Reichardt, *Chem. Rev*., 1994, **94**, 2319.
14. S. Das, S. Kundu, B. Sk, M. Sarkar and A. Patra, *Org. Mater*., 2021, **3**, 477.
15. D. Sasikumar, A. T. John, J. Sunny and M. Hariharan, *Chem. Soc. Rev*., 2020, **49**, 6122-6140.
16. R. Hu, E. Lager, A. Aguilar-Aguilar, J. Liu, J. W. Y. Lam, H. H. Y. Sung, I. D. Williams, Y. Zhong, K. S. Wong, E. Peña-Cabrera and B. Z. Tang, *J. Phys. Chem. C*, 2009, **113**, 15845-15853.
17. H. Uoyama, K. Goushi, K. Shizu, H. Nomura and C. Adachi, *Nature*, 2012, **492**, 234.
18. N. Notsuka, H. Nakanotani, H. Noda, K. Gousji and C. Adachi, *J. Phys. Chem. Lett*. 2020, **11**, 562.
19. L. Zhang, F. Jiang, Y. Liu and P. Jiang, *J. Phys. Chem. Lett.*, 2022, **13**, 3462.
20. X. Li, X. Liang, J. Yin and W. Lin, *Chem. Soc. Rev*., 2021, **50**, 102.
21. Q. Chen, H. Fang, X. Shao, Z. Tian, S. Geng, Y. Zhang, H. Fan, P. Xiang, J. Zhang, X. Tian, K. Zhang, W. He, Z. Guo and J. Diao, *Nat. Commun*., 2020, **11**, 6290.
22. H. Zhang, L. Shi, K. Li, X. Liu, M. Won, Y. Z. Liu, Y. Choe, X. Y. Liu, Y. H. Liu, S. Y. Chen, K. K. Yu, J. S. Kim and X. Q. Yu, *Angew. Chem. Int. Ed.*, 2022, **61**, e202116439.
23. J. Hong, Q. Li, Q. Xia and G. Feng, *Anal. Chem*., 2021, **93**, 16956.
24. X. Chao, Y. Qi and Y. Zhang, *ACS Sens*., 2021, **6**, 786.
25. S. Qi, S. Kim, V. Nguyen, Y. Kim, G. Niu, G. Kim, S. Kim, S. Park and J. Yoon, *ACS Appl. Mater. Interfaces*, 2020, **12**, 51293.
26. Q. Zhang, S. Xu, M. Li, Y. Wang, N. Zhang, Y. Guan, M. Chen, C. Chen and H. Hu, *Chem. Commun*., 2019, **55**, 5639-5642.